Nonlinear Dynamics (2026) 114:1017
https://doi.org/10.1007/s11071-026-12758-4

RESEARCH

The effect of different parametrizations including the perturbation of parameters on the energy transfer in a binary tree-structured mass–spring–damper system with nonlinear energy sinks

Róbert Rochlitz[1] · Bendegúz Dezső Bak[1]

Received: 28 November 2025 / Revised: 22 May 2026 / Accepted: 12 June 2026 / Published online: 7 August 2026

Abstract
The behavior of a multi-degree-of-freedom nonlinear oscillator arranged in a self-similar binary tree structure is studied for different parametrizations of its block masses and spring stiffnesses. The block masses of the oscillator are connected by linear springs across the levels of the tree, with the exception of the leaves of the tree, which are conventional nonlinear energy sinks. The main goal of the analysis is to investigate the potential of the oscillator to dissipate its energy content rapidly. The energy is fed to the oscillator via impulsive excitations. While nonlinear energy sinks perform well over a broad range of vibrational frequencies, they are sensitive to the input energy magnitude. We study how this sensitivity can be reduced by modifying the parametrization of the oscillator. Parametrizations with a small perturbation of the block masses are also considered. It is shown that the dissipation of the baseline parametrization can be improved by significantly decreasing the masses of the attached nonlinear energy sinks. However, this modification limits the effectiveness to a narrow range of smaller input energies. In contrast, for softer connections and lighter block masses across all levels of the tree, the nonlinear energy sinks provide consistently high dissipation over a much broader range of input energy, facilitated by efficient initial nonlinear beats followed by fundamental targeted energy transfer. The small perturbations of the block masses also improve the dissipation rate in general, but their effectiveness diminishes as the energy content increases. The difference between the unperturbed and perturbed cases is attributed to the separation of nonlinear normal modes with a multiplicity greater than one. These separated modes are involved in complex chaotic interactions, this is confirmed by the calculation of the largest Lyapunov exponent for each case.

1 Introduction

Nonlinear dynamical systems may exhibit a wide range of phenomenon not found in linear systems. For instance, targeted energy transfer (TET) is one such phenomenon, defined as a one-way and irreversible dynamical process in which the energy of the dynamical system is passed from one specific part (source) of the system to another (receiver) [1]. The complexity of TET arises from the strong, essential nonlinearities incorporated in the system that are required to trigger TET. Moreover, the process of TET is inherently transient. Dynamical systems with nonlinear energy sinks (NES) can exhibit TET. A NES is an essentially nonlinear dissipative attachment that can efficiently dissipate energy over a broad range of vibrational frequency [2]. The significance of TET is that the phenomenon provides a means for passive vibration control, e.g., to effectively mitigate undesirable vibrations in engineering systems [3–6], or to harvest energy [7–9]. Hence, the use of NESs makes it possible to quickly transfer and ultimately dissipate or harvest the vibrational energy of the system [10]. While some nonlinear systems are robust in the sense that their behavior is not sensitive for slight changes in their parameters or inputs [11, 12], others show high sensitivity. For example, a mechanical oscillator with a NES is sensitive to the initial energy of the system [13]. In particular, NESs require a threshold input energy (or excitation amplitude) to be activated [2].

The simplest NES consists of a lightweight mass attached to the primary system with a weak linear damper and a cubic nonlinear spring, this combination ensures efficient and irre-

✉ Róbert Rochlitz
rochlitzr@edu.bme.hu

Bendegúz Dezső Bak
bak.bendeguz@gpk.bme.hu

[1] Department of Fluid Mechanics, Faculty of Mechanical Engineering, Budapest University of Technology and Economics, Műegyetem rkp. 3., H-1111 Budapest, Hungary

versible transfer of energy — in other words TET — toward the NES that rapidly dissipates this energy [14, 15]. Recently other types of NESs were also introduced, for example, the bistable NES and the vibro-impact NES [16]. The bistable NES has a negative linear stiffness, hence, it has two stable and an unstable equilibria. The study of bistable NES drew attention, because it reduces significantly the input energy or excitation amplitude threshold that is required to activate the NES [17–19]. The vibro-impact NES aims to achieve similar improvements as the bistable NES. Instead of introducing negative linear stiffness, the vibro-impact NES consists of two masses attached to the primary system with a linear damper and a linear spring. The larger mass is a hollow body, there is a cavity inside of it. The smaller mass is put into this cavity and it can slide freely between the two ends of the cavity, impacting either end of this cavity. The impacts result in energy dissipation provided that the coefficient of restitution is smaller than unity [20–22].

A limitation of many studies in the topic is that they consider simple one to three degree-of-freedom (DoF) systems with a 1-DoF NES, while multi-DoF (MDoF) systems with multiple NESs also promise intriguing dynamics. For instance, Chen et al. [23, 24] demonstrated that the response of a dynamical system with multiple NESs can become chaotic for sufficiently large excitation amplitude. In their studies multiple NESs were attached to the primary linear system in a sequential arrangement and the primary linear system was excited with harmonic forcing. They showed that the response of the system is chaotic for some frequency bands, if the excitation amplitude is large enough. The arising chaotic dynamics triggered a very efficient TET within the chaotic bands compared to the frequencies outside of these bands. In the seminal book by Vakakis et al. [10] it is demonstrated that MDoF NESs are capable of interacting with multiple modes simultaneously, whereas a SDoF NES engages with modes of gradually lower frequency in a sequential manner, this is called a resonance capture cascade. Da Silva and Marques [25] examined a MDoF NES attached to a sprung cylinder which was subjected to vortex-induced vibrations. They demonstrated that by reducing the linear stiffness of the coupling between the NES and the linear oscillator, the amplitudes of the emergent limit cycle oscillations could be better controlled. Liu et al. [26] investigated the behavior of a MDoF NES exhibiting geometric nonlinearity in its springs and dampers, connected to a 1-DoF linear oscillator. When subjected to sufficiently high level of shock-energy, the resulting NES was capable of rapidly dissipating the energy. Kumar et al. [27] designed a 2-DoF NES using particle swarm optimization and showed that it outperforms the corresponding 1-DoF NES for large excitation amplitudes. A 2D inerter-enhanced NES capable of multi-directional vibration suppression was studied by Yang et al. [28]. Their proposed NES configuration was found to provide better vibration reduction for low-frequency vibrations compared to a similar 1-DoF inerter-enhanced NES. Zhang et al. [29] also found that under the same parameters, a well-designed 2-DoF NES has better dissipation than a 1-DoF NES.

In this study the qualitative behavior of a nonlinear MDoF mechanical oscillator is analyzed that is subjected to impulsive excitations. The investigated system is a binary tree-structured oscillator in which the block masses are connected by springs and dampers (Figure 1), allowing for additional vibrational modes not present in a simple chain oscillator. Similar structures were studied by Loong et al. [30], who examined the model properties of monopodial tree-structured linear oscillators, and Kovacic et al. [31], who investigated the localization that occurs in a binary tree-structured oscillator with both linear springs and springs with cubic nonlinearity.

The original idea for the proposed binary tree-structured system was to fabricate a mechanistic model based on the vortex breakdown in turbulent flows proposed by Richardson [32], and later theoretically studied in detail by Kolmogorov [33]. This idea has already motivated research preceding ours [34]. Further investigation into the connection between turbulence and mechanical vibrations was carried out by Boudaoud et al. [35], who studied the emergence and the properties of wave turbulence in a vibrating plate.

According to Richardson's eddy hypothesis [32] the turbulent energy cascade is formed by eddies of different scales who pass their kinetic energy to gradually smaller eddies. This energy cascade is sustained by the production of large vortices that are unstable and eventually break up into smaller vortices. This process goes on until the kinetic energy of the smallest vortices is dissipated due to the viscosity of the fluid. Therefore, the masses of the blocks in the tree also cover a vast range of scales, i.e., the masses of the blocks quickly decrease as the tree branches. We note that this study is not intended to establish an analogy between the characteristics of the turbulent energy cascade and those of the TET occurring in the investigated binary tree-structured oscillator. Instead, we focus on the potential of this binary tree-structured oscillator equipped with NESs to dissipate vibrational energy. The series of studies began with a purely linear version of this binary tree-structured oscillator [36, 37]. The energy distribution across the levels of the tree was derived analytically for the steadily decaying phase of the vibration, when the initial transients already died out. The characteristic polynomial was derived for a wide range of parametrizations of the tree, and the eigenvalue distribution was determined for a specific value of the scaling parameter, which prescribes how the masses of the blocks and the spring stiffnesses change for subsequent levels. In a follow-up study essential nonlinearity was added to the binary tree-structured oscillator by switching the linear tuned mass dampers (TMD) to NESs in the bottom level of the tree [38]. As opposed to the system reported in Chen et al. [23], the NESs are placed in a parallel arrangement in this binary tree-structured oscillator. The behavior of the system was analyzed for different types of impulsive and harmonic excitations with varying input energy and excitation amplitude. When TET developed in the system, the underlying driving mechanisms were identified and discussed. For the harmonic forcing, chaotic frequency bands similar to those reported in [23] were detected, though it was not formally proven that the dynamics was indeed chaotic within these frequency bands.

In this paper we first consider *unperturbed systems*, in which the masses of the blocks, spring stiffnesses, and damping coefficients do not change within a level. Then, we *mistune* the masses of the blocks, i.e., we draw a mistuned mass from a uniform distribution centered around the baseline value for each block. Thus, the masses of the blocks become slightly or moderately perturbed, depending on the width of the uniform distribution, creating a *perturbed system*. As it was demonstrated in a previous study [37], the mistuning process significantly alters the largest eigenvalues of the corresponding linear model, and it is capable of considerably changing the behavior of the system for certain initial conditions. Our goal is to find changes in the behavior of the perturbed systems compared to the unperturbed system, and relate these changes to the mistuning. The effects of this perturbation of the masses on energy transfer mechanisms and the degree of chaos is examined through wavelet transforms (WTs) [39, 40] in frequency energy plots (FEP) [41, 42] and Lyapunov exponents [43]. It is demonstrated that this mistuning of the masses of the system can significantly change the behavior of the model for small initial energies, whereas its effects diminish for larger initial energies. We further show — by numerical calculation of the largest Lyapunov exponent — that the perturbed systems tend to be considerably more chaotic than their respective unperturbed version.

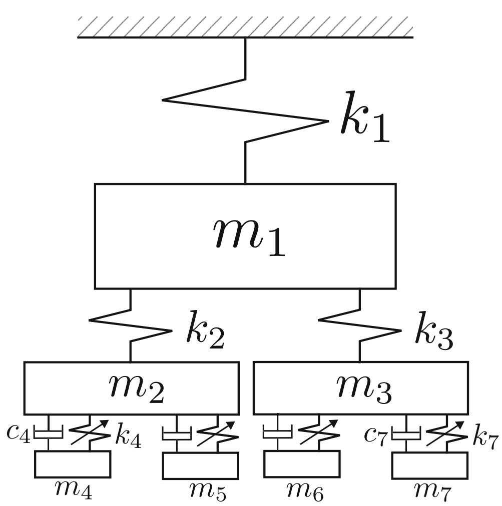

Fig. 1 The binary tree-structured nonlinear oscillator with 3 levels

This paper is structured as follows. In Section 2 the MDoF nonlinear binary tree-structured oscillator is introduced, the parametrization of the system, including the mistuned parameters, is discussed. In Section 3 the methodology and tools are introduced that are used to evaluate the results of the study. The simulation results for different parametrizations of the model are provided in Section 4 for some representative initial conditions. The results focus on demonstrating the effects of the mistuning and comparing the behavior of the systems having different parametrizations. Finally, conclusions are drawn in Section 5.

2 Model description

2.1 The binary tree-structured oscillator

An n-level binary tree of block masses m_i connected by linear and nonlinear springs k_i and dampers c_i is considered, an example with three levels is shown in Fig. 1. In this system the blocks are connected with linear springs across all levels, except the last two levels where the connection is provided by dampers and cubic nonlinear springs. Thus, the bottom level of the tree consists of NESs. The tree has n levels, level $l = 1, \ldots, n$ consists of 2^{l-1} blocks, thus, the total number of blocks is $N = 2^n - 1$. The top block of mass m_1 is connected to a fixed wall with a spring whose stiffness is k_1. Throughout this study, every quantity is considered to be dimensionless.

The equations of motion can be written in a general form for a system consisting of $n \geq 3$ levels as

$$
\begin{aligned}
m_i\ddot{x}_i &= -k_i x_i + k_{2i}(x_{2i} - x_i) + k_{2i+1}(x_{2i+1} - x_i), \quad i = 1,\\
m_i\ddot{x}_i &= k_i(x_{\lfloor i/2\rfloor} - x_i) + k_{2i}(x_{2i} - x_i)\\
&\quad + k_{2i+1}(x_{2i+1} - x_i), \quad i \in \mathcal{I}(l),\ l = 2, \ldots, n-2,\\
m_i\ddot{x}_i &= k_i(x_{\lfloor i/2\rfloor} - x_i) + k_{2i}(x_{2i} - x_i)^3\\
&\quad + k_{2i+1}(x_{2i+1} - x_i)^3 + c_{2i}(\dot{x}_{2i} - \dot{x}_i)\\
&\quad + c_{2i+1}(\dot{x}_{2i+1} - \dot{x}_i), \quad i \in \mathcal{I}(n-1),\\
m_i\ddot{x}_i &= k_i(x_{\lfloor i/2\rfloor} - x_i)^3 + c_i(\dot{x}_{\lfloor i/2\rfloor} - \dot{x}_i), \quad i \in \mathcal{I}(n),
\end{aligned}
\tag{1}
$$

with initial conditions (ICs)

$$x_i(0) = x_{i,0}, \quad \dot{x}_i(0) = v_{i,0}, \quad i = 1, \ldots, N, \tag{2}$$

where $\mathcal{I}(l) = \{2^{l-1}, \dots, 2^l - 1\}$ is the set of indices corresponding to level l, $x_i \equiv x_i(t)$ is the displacement of block i, and t is the time. The initial conditions $x_{i,0}$, $v_{i,0}$ are the initial displacement and velocity of block i, respectively. The notation $\lfloor \cdot \rfloor$ denotes the floor operation, and the notation $(\dot{\cdot})$ stands for the derivative with respect to time.

Then, the system of differential equations (1) and ICs (2) in matrix form are

$$\mathbf{M}\ddot{\mathbf{x}}(t) + \mathbf{C}\dot{\mathbf{x}}(t) + \mathbf{K}_1\mathbf{x}(t) + \mathbf{K}_2(\mathbf{x}(t)) = \mathbf{0}, \quad \mathbf{x}(0) = \mathbf{x}_0, \quad \dot{\mathbf{x}}(0) = \mathbf{v}_0, \tag{3}$$

where $\mathbf{x}(t)$ is the vector of displacements, $\mathbf{M}$, $\mathbf{C}$, and $\mathbf{K}_1$ are the mass, damping, and stiffness matrices, respectively. The vector $\mathbf{K}_2(\mathbf{x}(t))$ contains the terms of Eq. (1) with cubic nonlinearities. The vectors $\mathbf{x}_0$ and $\mathbf{v}_0$ consist of the initial displacements and velocities of the blocks, respectively. Without formally performing the nondimensionalization of Eq. (3), we will treat this equation as nondimensional and fix the values $m_1 = 1$ and $k_1 = 1$.

2.2 The energy of the system

The total energy $E(t)$ of the system Eq. (1) is calculated as

$$\begin{aligned} E(t) =& \frac{1}{2}\dot{\mathbf{x}}(t)^{\mathrm{T}}\mathbf{M}\dot{\mathbf{x}}(t) + \frac{1}{2}\mathbf{x}(t)^{\mathrm{T}}\mathbf{K}_1\mathbf{x}(t) \\ &+ \frac{1}{4}\sum_{i\in\mathcal{I}(n)} k_i(x_i(t) - x_{\lfloor i/2 \rfloor}(t))^4. \end{aligned} \tag{4}$$

The dissipation rate $\varepsilon(t)$ of the system Eq. (1) is defined as the rate of change of the total energy Eq. (4) multiplied by -1, i.e.,

$$\varepsilon(t) = -\dot{E}(t). \tag{5}$$

We also consider the $E_l(t)$ energy stored in level l (level energy) of the system Eq. (1), which is defined such that the potential energy of a spring is evenly distributed amongst the masses connected to it, hence,

$$\begin{aligned} E_l(t) =& \frac{1}{2}\sum_{i\in\mathcal{I}(l)} m_i \dot{x}_i^2(t) \\ &+ \frac{1+\delta_{l,1}}{4(1+\delta_{l,n})}\sum_{i\in\mathcal{I}(l)} k_i(x_i(t) - x_{\lfloor i/2 \rfloor}(t))^{2(1+\delta_{l,n})} \\ &+ \frac{1}{4(1+\delta_{l,n-1})}\sum_{i\in\mathcal{I}(l+1)} k_i(x_i(t) - x_{\lfloor i/2 \rfloor}(t))^{2(1+\delta_{l,n-1})}, \\ & l = 1, \dots, n, \end{aligned} \tag{6}$$

where δ is the Kronecker delta. Note that the sum of these level energies results the total energy $E(t)$ of the system Eq. (1), i.e.,

$$E(t) = \sum_{l=1}^{n} E_l(t). \tag{7}$$

2.3 Model parameters

By design, dampers are incorporated only between the blocks of the last two levels. The masses of the blocks and the stiffnesses of the springs in the system are considered to follow a simple power-law, while the damping coefficient of the dampers in the bottom level have a fixed value, i.e.,

$$\begin{aligned} m_i &= \frac{M_l}{\mu^{\delta_{l,n}}} = \frac{\sigma^{l-1}}{\mu^{\delta_{l,n}}}, \quad i \in \mathcal{I}(l), \quad l = 1, \dots, n, \\ k_i &= K_l = \sigma^{l-1}, \qquad i \in \mathcal{I}(l), \quad l = 1, \dots, n, \\ c_i &= 0, \qquad i \in \mathcal{I}(l), \quad l = 1, \dots, n-1, \\ c_i &= c = 0.001, \qquad i \in \mathcal{I}(n). \end{aligned} \tag{8}$$

Thus, the parameters on a given level l are the same. The term M_l denotes the “mass scale” representing the mass of each block in level $l = 1, \dots, n$. The quantity K_l refers to the stiffness of every spring connecting the blocks of the $l-1$th and lth levels. The damping coefficient of every damper is simply denoted by c and fixed to be $c = 0.001$, as a weak damping is a necessary condition of the emergence of passive TET [10]. The symbol δ stands for the Kronecker delta.

The quotient $\sigma > 0$ of the power-law is the *scaling parameter*, that defines the masses of the blocks and the stiffnesses of the springs on each level. As we stated in the introduction and the description of the system, we require decreasing block masses for subsequent levels, which limits the choice of the quotient to $0 < \sigma < 1$. The NESs must also be lightweight compared to the total mass of the system to ensure the realization of efficient TET [10]. Further limiting the quotient to $0 < \sigma \leq 0.5$ ensures that the sum of the block masses also does not increase for subsequent levels. The choice of $\sigma = 0.5$ is special, since the sum of the block masses as well as the sum of the spring stiffnesses add up to exactly 1 within each level. Hence, $\sigma = 0.5$ defines the baseline system for our investigation.

In [44] it was demonstrated that reducing the stiffness of the spring connecting a NES to a linear oscillator increases the energy fraction contained in the NES. In order to extend this investigation to a MDoF linear oscillator with multiple NESs, we also consider the case of $\sigma = 0.4$ for thorough study. This yields a softer and lighter system compared to the baseline system.

It is heavily emphasized by Gendelman et al. [45] and also thoroughly discussed in [10] that the NESs must be lightweight compared to the total mass of the oscillator, which inspired an idea to further decrease the mass of the

NES blocks. This is the role of the parameter $\mu \geq 1$ in Eq. (8). The masses of the NES blocks are further reduced, when $\mu > 1$ is chosen. In the baseline case $\mu = 1$ is kept, i.e., the masses of the NES blocks precisely follow the power-law that is prescribed by the scaling parameter σ. In a modified system we set $\mu = 4$ to have significantly lighter NES blocks compared to the baseline system.

The system Eq. (1) that completely obeys the parametrization given in Eq. (8) is called the *unperturbed system* throughout this study. We also consider *perturbed systems* (or mistuned systems), where perturbation of the block masses m_i with parameter r is introduced as

$$m_i \sim \mathcal{U}[(1-r)M_l, (1+r)M_l], \quad i \in \mathcal{I}(l), \quad l = 1, \ldots, n, \tag{9}$$

where $\mathcal{U}$ denotes the continuous uniform distribution, and $r \in (0, 1]$ is the mistuning parameter. While we acknowledge that the parameters of real life engineering systems rather exhibit normal distribution around their design values, our goal is simply to investigate whether perturbing the block masses has any significant effect on the dynamics. The masses of the blocks are perturbed with small to moderate extent in this study. In particular, the range of mistuning parameters $r \in [0.01, 0.1]$ is investigated.

3 Methodology

We consider unperturbed systems described by the equations of motion Eq. (1) and ICs Eq. (2) with parameters Eq. (8), and perturbed systems in which the block masses are mistuned according to Eq. (9). First, we compare the response of the unperturbed systems with different parameters. Then, we look for significant changes in the behavior of the perturbed systems compared to their respective unperturbed system to showcase the effect of the mistuning. To do this, we identify the energy transfer mechanisms in the investigated unperturbed and perturbed systems, and determine how the initial energy content and the mistuning of the masses affect these mechanisms.

The initial energy content of the system Eq. (1) is determined by the initial conditions Eq. (2). The idea is to feed the initial energy to the system at the top of the tree and realize a transfer of energy from the top blocks having the largest masses toward the smaller ones, similarly to an energy cascade. We expect the development of a highly efficient, irreversible transfer of the vibrational energy toward the NESs, which constitute the leaves of the tree. Hence, we prescribe the ICs as

$$\begin{aligned}
&x_i(0) = 0, \quad i = 1, \ldots, N, \\
&\dot{x}_1(0) = v_{1,0}, \quad \dot{x}_2(0) = v_{2,0}, \quad \dot{x}_3(0) = v_{3,0}, \\
&\dot{x}_i(0) = 0, \quad i = 4, \ldots, N,
\end{aligned} \tag{10}$$

where $v_{1,0}$, $v_{2,0}$, and $v_{3,0}$ are the initial velocities of the top three blocks. Thus, the initial position of every block is zero, as well as the initial velocity of every block, except the top three blocks, which have the largest masses. With this set of ICs the initial energy $E_0 \equiv E(0)$ of the system is

$$E_0 = E_1(0) + E_2(0) = \frac{1}{2}\left(m_1 v_{1,0}^2 + m_2 v_{2,0}^2 + m_3 v_{3,0}^2\right). \tag{11}$$

Depending on the actual choice of $v_{1,0}$, $v_{2,0}$, and $v_{3,0}$ different modes of the system Eq. (1) can be excited. We investigate whether there is a significant change in the dynamic behavior of the system due to the change of ICs for a fixed initial energy content E_0.

The energy would decay exponentially in a linear oscillator with TMDs. NESs also allow faster than exponential energy decay [46], provided the initial energy is sufficiently high to trigger strongly nonlinear dynamics. Then, we can identify the time periods of TET as the time intervals where the total energy $E(t)$ of the system decays faster than exponential. It is convenient to plot $E(t)$ as the function of time t on a logarithmic scale. For exponential decay, the graph of $\log E(t)$ is linear, whereas it is concave for faster than exponential decay. This means that one can identify the time intervals associated with TET on the graph of $\log E(t)$ as function of the time t. The onset as well as the end of TET will be marked by inflection points.

In Fig. 2 we depict such a logarithmic plot of the total energy $E(t)$ for a realization of the perturbed ($r = 0.02$) baseline system ($\sigma = 0.5$, $\mu = 1$) that consists of $n = 6$ levels. In this case an initial energy content of $E_0 = 5$ was prescribed with the initial conditions $v_{1,0} = \sqrt{10}$, $v_{2,0} = v_{3,0} = 0$. A characteristic behavior of such systems is the initial nonlinear beats, which end at the time marked by the dashed orange line. Up to this inflection point, the graph of $\log E(t)$ is concave, which demonstrates that initially we indeed have TET. The onset of another TET mechanism is at the next inflection point marked by the dashed green line, where the graph switches back to concave again. TET ceases at the subsequent inflection point marked by the dashed blue line. Then, the efficiency of the dissipation quickly degrades as the NESs deactivate. Another quantity of interest is the energy fraction stored in the NESs as function of the time, which shows the activation of the NESs. Graphical representation of elevated or even increasing energy content in the NESs nicely visualizes TET. The energy stored in the NESs

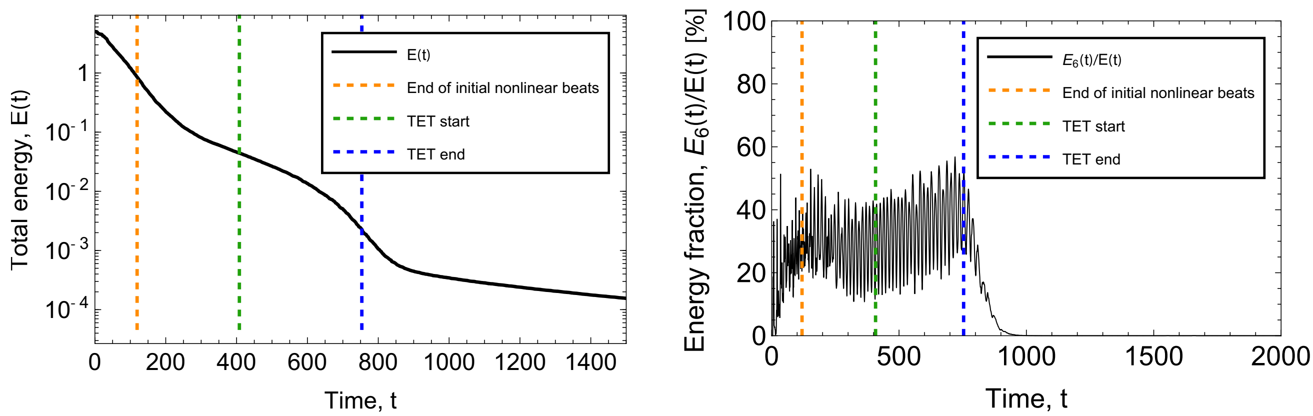

Fig. 2 Total energy $E(t)$ (left), and the fraction of the total energy stored in the NESs $E_6(t)/E(t)$ (right) of a perturbed system ($r = 0.02$) consisting of $n = 6$ levels with $\sigma = 0.5$, $\mu = 1$. The initial energy is $E_0 = 5$ with initial conditions $v_{1,0} = \sqrt{10}$, $v_{2,0} = v_{3,0} = 0$. The colored vertical dashed lines mark the the end of the initial nonlinear beats, then the onset, and the end of another phase of TET

is captured by the level energy $E_6(t)$, hence we can analyze the energy fraction $E_6(t)/E(t)$ as function of the time t to identify different types of TET, as shown in Fig. 2.

Analogously to the vibrational modes of linear systems, nonlinear normal modes (NNMs) can be defined for nonlinear dynamical systems. A characteristic of NNMs is that their oscillation frequency depends on the total energy of the system. This dependency of the frequency of NNMs is captured by the FEP of the system [10], which is shown in Fig. 3 for the unperturbed baseline system ($\sigma = 0.5$, $\mu = 1$). Here the horizontal thin black and dashed blue lines mark the eigenvalues of the underlying linear systems obtained by omitting the nonlinear springs (setting them to $k_i = 0$ for $i \in \mathcal{I}(n)$) or replacing them with rigid rods (setting them to $k_i \to \infty$ for $i \in \mathcal{I}(n)$), respectively. The thick red lines — known as *backbone curves* — show the 1:1 NNMs, in which all the blocks exhibit the same oscillation frequency ω. The backbone curves are separated by the eigenvalues of the underlying linear systems. Of these NNMs, the bottom branch in Fig. 3 covering the lowest frequency range is of particular interest, as it corresponds to the in-phase 1:1 NNM, meaning that every block oscillates in-phase relative to each other. The backbone curves were obtained using the harmonic balance method [47], in which the motion of the block masses was assumed to follow the equation

$$x_i(t) = A_i \cos(\omega t), \quad i = 1, \dots, N, \tag{12}$$

where $\omega \in [0, 2.5]$ is the angular frequency and A_i is the amplitude corresponding to block i. After substituting Eq. (12) into the equation of motion Eq. (1) and performing simplifications, the $\cos(\omega t)$ terms were matched. The resulting system of equations is solved numerically for the A_i amplitudes in the angular frequency range $\omega \in [0, 2.5]$. Finally, the total energy is calculated from the amplitudes A_i in accordance with Eq. (4).

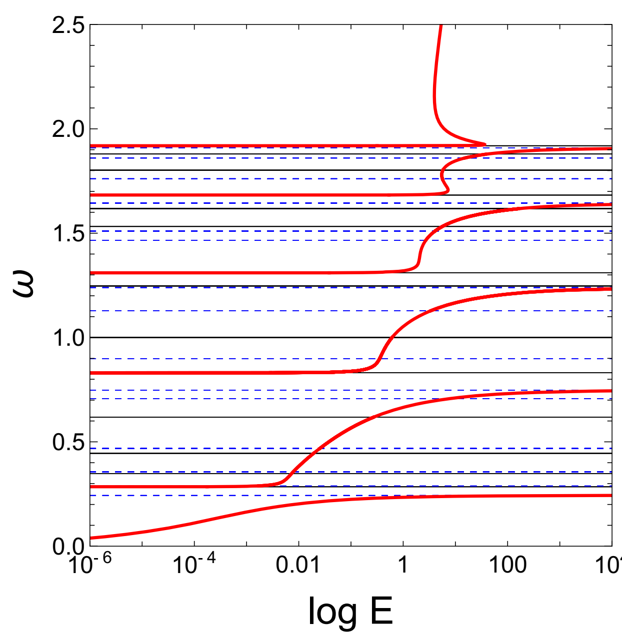

Fig. 3 Frequency energy plot of the unperturbed and undamped system ($\mathbf{C} = \mathbf{0}$) described by the equations of motion Eq. (1) with $n = 6$ levels, and $\sigma = 0.5$, $\mu = 1$. The thick red lines show the 1:1 NNMs. The horizontal thin black and dashed blue lines show the eigenvalues of the underlying linear systems obtained by setting $k_i = 0$ and $k_i \to \infty$ ($i \in \mathcal{I}(n)$)

Changing the parametrization of the system alters the FEP. In particular, decreasing the scaling parameter σ narrows the frequency range occupied by the eigenvalues of the underlying linear systems, hence the FEP is “squeezed” vertically. Increasing the scaling parameter σ has the opposite effect. When only the mass of the NES blocks are decreased leaving the other block masses and the spring stiffnesses unchanged

($\mu > 1$), the NNMs are shifted towards the left of the FEP. This latter modification has an important consequence that is discussed in Section 4.

The FEP is usually constructed for the undamped system ($c_i = 0$ for $i = 1, \ldots, N$ as opposed to what Eq. (8) specifies), but it also provides a sufficiently accurate approximation for the weakly damped version of the same system. The wavelet transform, which shows the frequency of the vibration as function of the energy content of the system, can be plotted onto the FEP as a contour plot (not shown in Fig. 3) to show which NNMs are active during the vibration. The WT is derived from displacement and energy time histories.

We can also investigate the potentially chaotic nature of the oscillation by means of approximation of the largest finite Lyapunov exponent λ_{max} based on the work of Kuptsov and Parlitz [43]. A positive Lyapunov exponent λ_{max} indicates that the dynamics of the system is chaotic, while the magnitude of the exponent describes the degree of chaos. Since the calculation method of Lyapunov exponents require non-decaying vibration and we do not have production in the form of an external excitation, we calculate the largest finite Lyapunov exponent λ_{max} for the undamped system. In order to corroborate the conclusions based on the largest Lyapunov exponents, phase portraits and Poincaré sections were also constructed for some representative cases with damping. While a 2D slice of the phase space with $2N$ dimensions cannot conclusively demonstrate chaos, nonetheless a phase portrait which "fills" a finite region of the phase space and a Poincaré section that consists of a scattered cloud of points are consistent with the irregular motion expected in a system where chaos is present.

4 Results

We consider the system Eq. (1) with $n = 6$ levels using the following three combinations of the parameters σ and μ in line with the considerations discussed in Section 2.3:

- The combination $\sigma = 0.5$ and $\mu = 1$ provides the *baseline* system of the investigations. Besides featuring the decreasing block masses for subsequent levels, the sum of the masses of the blocks also does not increase for subsequent levels. The NES blocks are lightweight enough (compared to the total mass of the system) to realize efficient TET.
- The combination $\sigma = 0.5$ and $\mu = 4$ yields the *modified* system, as it introduces a modification to the baseline system in which the mass of each NES block is reduced significantly. This modification allows us to further reduce the mass of the NES blocks without being bounded by the scaling parameter σ.
- The combination $\sigma = 0.4$ and $\mu = 1$ yields a *softening* system that becomes gradually lighter and softer toward the bottom of the three compared to the baseline system. Based on the literature, we expect that using both lightweight blocks and soft springs facilitate efficient energy transfer from the linear part of the system towards the NES blocks.

The following combinations of ICs obeying Eq. (10) are prescribed for the unperturbed systems:

- $v_{1,0} > 0$, $v_{2,0} = v_{3,0} = 0$. *Simple IC*, meaning that only the initial velocity of the top, largest block is nonzero.
- $v_{1,0} > 0$, $v_{2,0} = v_{3,0} > 0$. *In-phase IC*, meaning that the top three blocks are pushed in the same direction. Moreover, the initial energy is distributed equally between the first two levels of the system, i.e., $E_1(0) = E_2(0)$.
- $v_{1,0} > 0$, $v_{2,0} > 0$, $v_{3,0} < 0$, $|v_{2,0}| = |v_{3,0}|$. *Mixed IC*, meaning that the two blocks of the second level are pushed in the opposite direction, but with the same magnitude. Again, the initial energy is distributed equally between the first two levels of the system, i.e., $E_1(0) = E_2(0)$.

The condition $E_1(0) = E_2(0)$ for the in-phase IC and mixed IC cases is fulfilled for unperturbed systems, when $|v_{2,0}| = |v_{3,0}| = \sqrt{1/(2\sigma)}v_{1,0}$.

A set of numerical simulations are carried out providing different initial energies in the range $E_0 \in [0.2, 50]$ for the unperturbed systems with the above described combinations of the initial velocities $v_{1,0}$, $v_{2,0}$, $v_{3,0}$. Then, the simulations are repeated with perturbed systems. In each simulation, the value E_0 is precisely prescribed, i.e., the initial velocities $v_{1,0}$, $v_{2,0}$, $v_{3,0}$ of the top three blocks are adjusted to compensate the mistuned values of m_1, m_2, m_3. For the in-phase IC and mixed IC $E_1(0) = E_2(0)$ is also kept, moreover, $E_2(0)$ is equally distributed between the blocks of the second level, meaning $m_2 v_{2,0}^2 = m_3 v_{3,0}^2$. The results of perturbed systems are presented in detail for $r = 0.05$, as we found that the mistuning itself has a significant impact, but its extent is of less importance in the investigated range of mistuning parameters $r \in [0.01, 0.1]$.

4.1 Dynamics with simple IC

In this case the top block has a nonzero initial velocity, every other IC is zero. The total energy $E(t)$ time histories of some perturbed (with $r = 0.05$) systems and those of the unperturbed systems are shown in Fig. 4 for initial energies $E(0) = 1$ and $E(0) = 5$. Though these results do not show convincingly that any parametrization of the unperturbed systems is in general superior to the other two in terms of energy dissipation, the overall conclusion will be different

Fig. 4 Comparison of the total energy $E(t)$ for the three different parametrizations of some perturbed ($r = 0.05$) and the unperturbed systems with the simple IC for initial energies $E_0 = 1$ and $E_0 = 5$

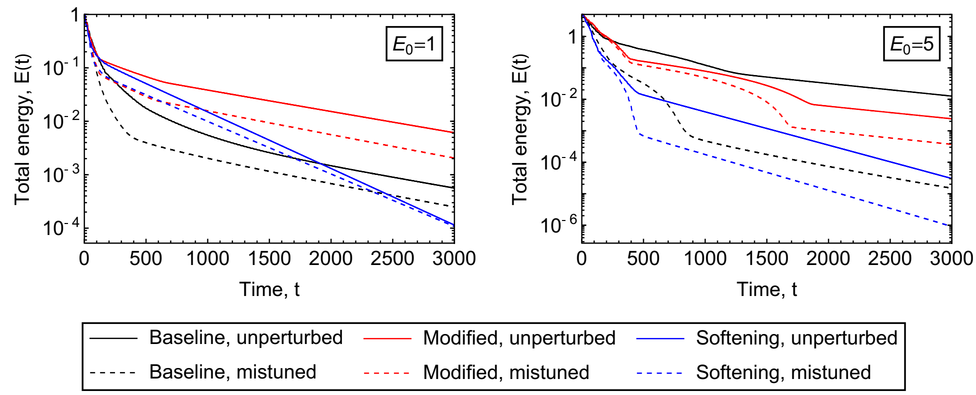

once all results of Section 4 are assessed. At this point one can observe that the introduction of mass mistuning increases the energy dissipation rate in the investigated cases, though the significance of this effect greatly varies depending on the parametrization and the initial energy of the system.

Though the modified system with lightweight NES blocks ($\sigma = 0.5$ and $\mu = 4$) outperforms the baseline system ($\sigma = 0.5$ and $\mu = 1$) in terms of dissipation for the higher initial energy content $E_0 = 5$, the latter has more potential to rapidly dissipate vibrational energy with mistuning. In Fig. 5 the total dissipation is shown up to some time t, which is expressed as the fraction of the dissipated energy $E_0 - E(t)$ of the system compared to its initial energy E_0, i.e., $(E_0 - E(t))/E_0$. In these charts each column represents an unperturbed (striped column) system, and the average result over 100 realizations of perturbed (filled column) systems. The connected dots indicate the standard deviation of the results corresponding to perturbed systems. When a filled column overlaps the striped column, it means that the perturbed systems on average exhibit equivalent or better performance in terms of dissipation compared to the unperturbed system. A striped column shown over the white background indicates the opposite.

One can see that the performance of the baseline system is equivalent or better in most cases compared to the modified system over the investigated initial energy range $E_0 \in [0.2, 50]$. On average, the perturbation also improves the performance of the baseline system more significantly. Meanwhile, the softening system ($\sigma = 0.4$ and $\mu = 1$) promotes high dissipation rate consistently that is practically unaffected by the perturbation.

In Figs. 6, 7, and 8 the energy fraction $E_6(t)/E(t)$ stored in the NES blocks and the WT of $x_{32}(t)$ (the displacement solution of a NES block) superimposed onto the FEP are shown for each investigated case with $E_0 = 5$. The black and red vertical lines mark the end of the initial nonlinear beats and the follow-up TET for the unperturbed system and a perturbed system, respectively. Fundamental TET does not develop after the initial nonlinear beats, which cease at the time marked by the first thick vertical line in the time histories. While the energy fraction stored in the NESs remains significant, it does not increase rapidly over time. The steady, non-increasing energy content stored in the NESs suggests that only weak subharmonic TET develops, which persists for a longer time compared to the initial nonlinear beats. This weak TET ceases at the time marked by the second thick vertical line. In these cases the WT plot shows that multiple

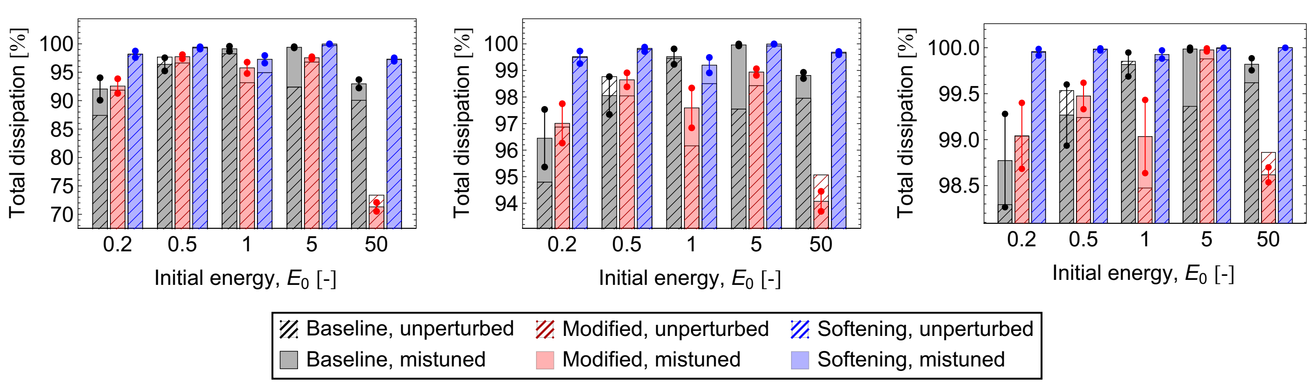

Fig. 5 Fraction of the dissipated initial energy of the system at $t = 500$ (left), $t = 1000$ (middle), and $t = 2000$ (right) as a function of the initial energy E_0 for the three different parametrizations of the unperturbed and the perturbed systems ($r = 0.05$) with simple IC

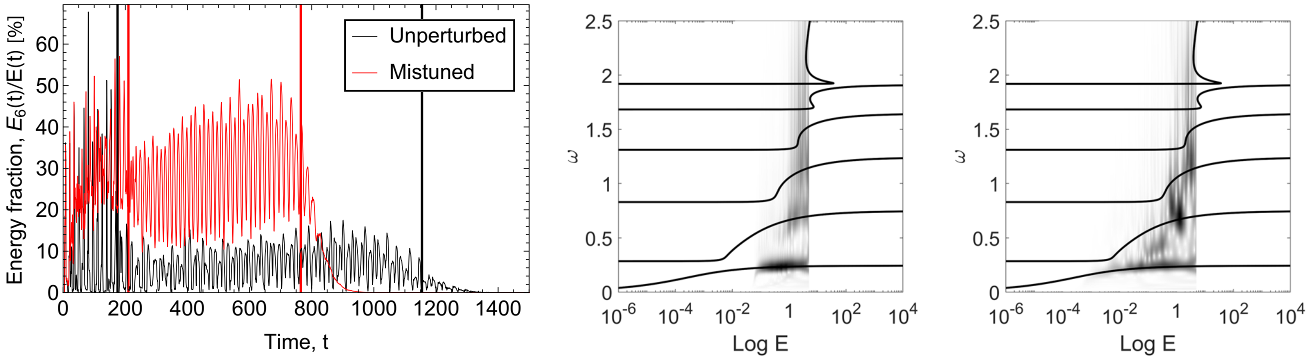

Fig. 6 Energy fraction $E_6(t)/E(t)$ stored in the last level (left), the corresponding WT of a NES block for the unperturbed system (middle), and the perturbed system with $r = 0.05$ (right) for the baseline system, with the simple IC and initial energy $E_0 = 5$

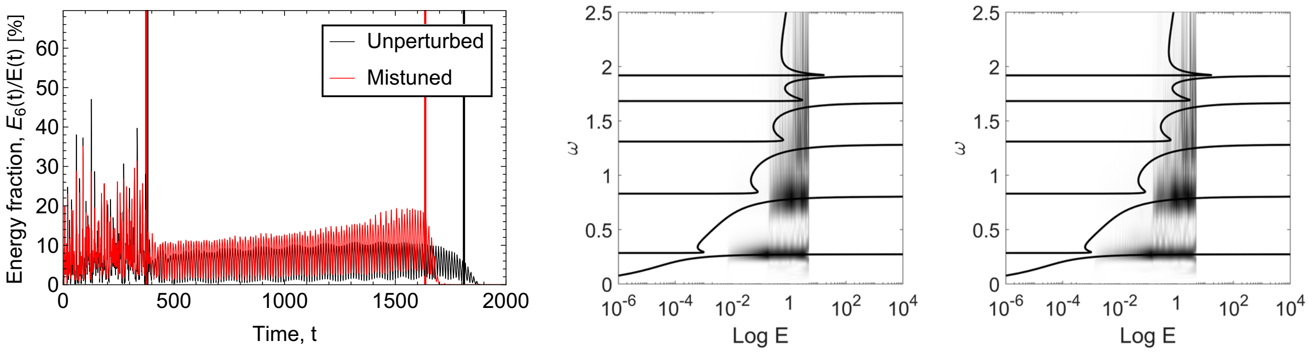

Fig. 7 Energy fraction $E_6(t)/E(t)$ stored in the last level (left), the corresponding WT of $x_{32}(t)$ for the unperturbed system (middle), and the perturbed system with $r = 0.05$ (right) for the modified system, with the simple IC and initial energy $E_0 = 5$

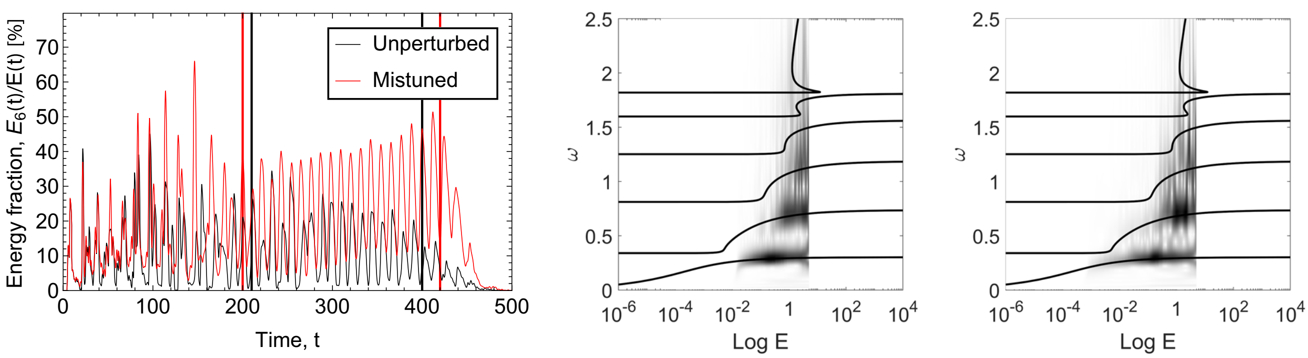

Fig. 8 Energy fraction $E_6(t)/E(t)$ stored in the last level (left), the corresponding WT of $x_{32}(t)$ for the unperturbed system (middle), and the perturbed system with $r = 0.05$ (right) for the softening system, with the simple IC and initial energy $E_0 = 5$

NNMs are excited simultaneously. This prevents clear 1:1 transient resonance capture that would yield stronger fundamental TET. While the in-phase NNM associated with the lowest vibration frequency in the FEP outlives the others in general, residual energy content in other higher frequency NNMs can still compromise resonance capture and force the system to escape TET.

In order to assess what is preventing 1:1 transient resonance capture, some displacement solutions $x_i(t)$ of the system must be picked for further analysis. In Fig. 9 the displacement solutions $x_{16}(t)$ and $x_{32}(t)$ as well as the corresponding energy spectral density (ESD) plots are depicted for the unperturbed baseline system during the second TET phase. In fact, the ESD plots of $x_{16}(t)$ and $x_{32}(t)$ rule out subharmonic TET as no oscillation frequency of fractional multiple of the main oscillation frequency is detected. However, a significant high frequency peak is present in the ESD of $x_{16}(t)$ which is also noticeable in the time history of $x_{16}(t)$. The same conclusions can be drawn for the modified and

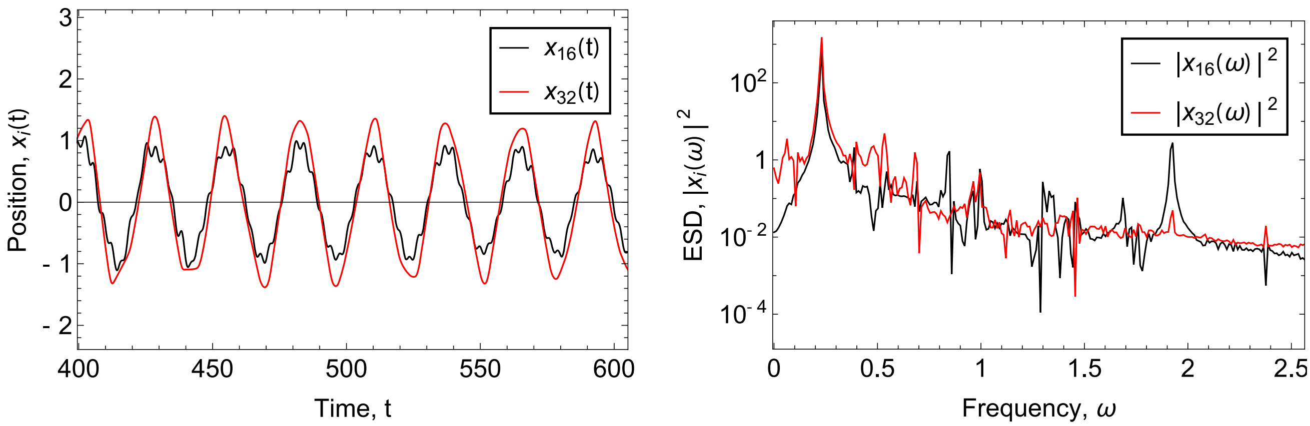

Fig. 9 Displacement solutions $x_{16}(t)$ and $x_{32}(t)$ (left) and the corresponding ESD of $x_{16}(t)$ and $x_{32}(t)$ (right) during the second TET phase for the unperturbed baseline system with the simple IC and initial energy $E_0 = 5$

softening systems upon the inspection of the respective displacement solutions.

For lower initial energy content (e.g., $E_0 = 1$), we can even lose the ability to produce the weak second TET phase. The NESs simply do not remain active once the initial nonlinear beats settle. This is indicated by Fig. 4, as for $E_0 = 1$ the graphs of $\log E(t)$ do not exhibit a second, longer concave segment, which is expected when any form of nonlinear TET kicks in after the initial nonlinear beats. The same graphs for $E_0 = 5$ showcase the concave segments that coincide with the time interval associated with the second TET phase.

The energy fraction $E_6(t)/E(t)$ stored in the NES blocks is consistently increased for the perturbed systems resulting in stronger dissipation. The WT plots suggest that the increased dissipation rate of the perturbed systems is facilitated by "split modes" and "hidden modes". The former are the repeated modes of the unperturbed system which fell apart due to the mistuning [37], while the latter are asymmetric modes that are difficult to access due to the symmetry of both the system parameters and the ICs in case of the unperturbed systems [48]. Altogether several additional modes are activated whose chaotic interaction results in a more efficient dissipation.

The largest Lyapunov exponents λ_{max} corresponding to each case shown in Fig. 10 agree. The λ_{max} values are positive in every case, and they are also consistently and significantly larger for the perturbed cases. Only results for $r = 0.05$ are showcased in the figure, since practically the same results were obtained for significantly smaller ($r = 0.01$) and larger ($r = 0.1$) mistuning parameters. This shows that the mistuning itself has a significant impact, but its extent is of less importance. In the perturbed cases, each data point in the figure represents average values over 100 realizations of the perturbed system. These findings indicate that perturbed systems exhibit more chaotic behavior compared to the unperturbed system regardless of the parametrization or the initial energy. In Fig. 10 representative phase portraits and Poincaré sections of the system with each parametrization are also depicted. The Poincaré sections were created as the intersection of the $x_1(t) = 0$ plane with the phase portrait, essentially marking the phase portrait every time the sign of $x_1(t)$ changed from positive to negative, i.e., $\dot{x}_1(t) < 0$. The phase portraits and Poincaré sections are drawn between the onset and end of the second TET phase (the phase between the vertical lines in Figs. 6, 7, and 8) to rule out the effect of the initial nonlinear beats. These phase portraits densely "fill" the phase space, while the accompanying Poincaré sections consist of irregular point clouds. Thus, both the phase portraits and the Poincaré sections indicate chaos that is consistent with the positive Lyapunov exponents.

Fig. 11 shows the total energy $E(t)$ for the same set of cases as Fig. 4 with a much larger initial energy of $E_0 = 50$. For the baseline and modified systems this high initial energy content clearly falls outside of the effective range of energy content in which the NESs could perform. On the other hand, the softening system exhibits a strong fundamental TET, resulting in much more efficient dissipation compared to the other two parametrizations. Fig. 12 confirms that fundamental TET develops in the softening system for $E_0 = 50$. The energy fraction stored in the NESs rapidly increases until $t \approx 1300$, where the cutoff happens and the system escapes the 1:1 transient resonance capture. We note that in this case the mistuning has no significant effect on the dynamics, which we found to be the general behavior of the system with high initial energy content regardless of the parametrization.

4.2 Dynamics for in-phase IC

In this case the top three blocks in the first two levels have a nonzero initial velocity, every other IC is zero. Moreover, the sign of the initial velocities is the same for these three blocks,

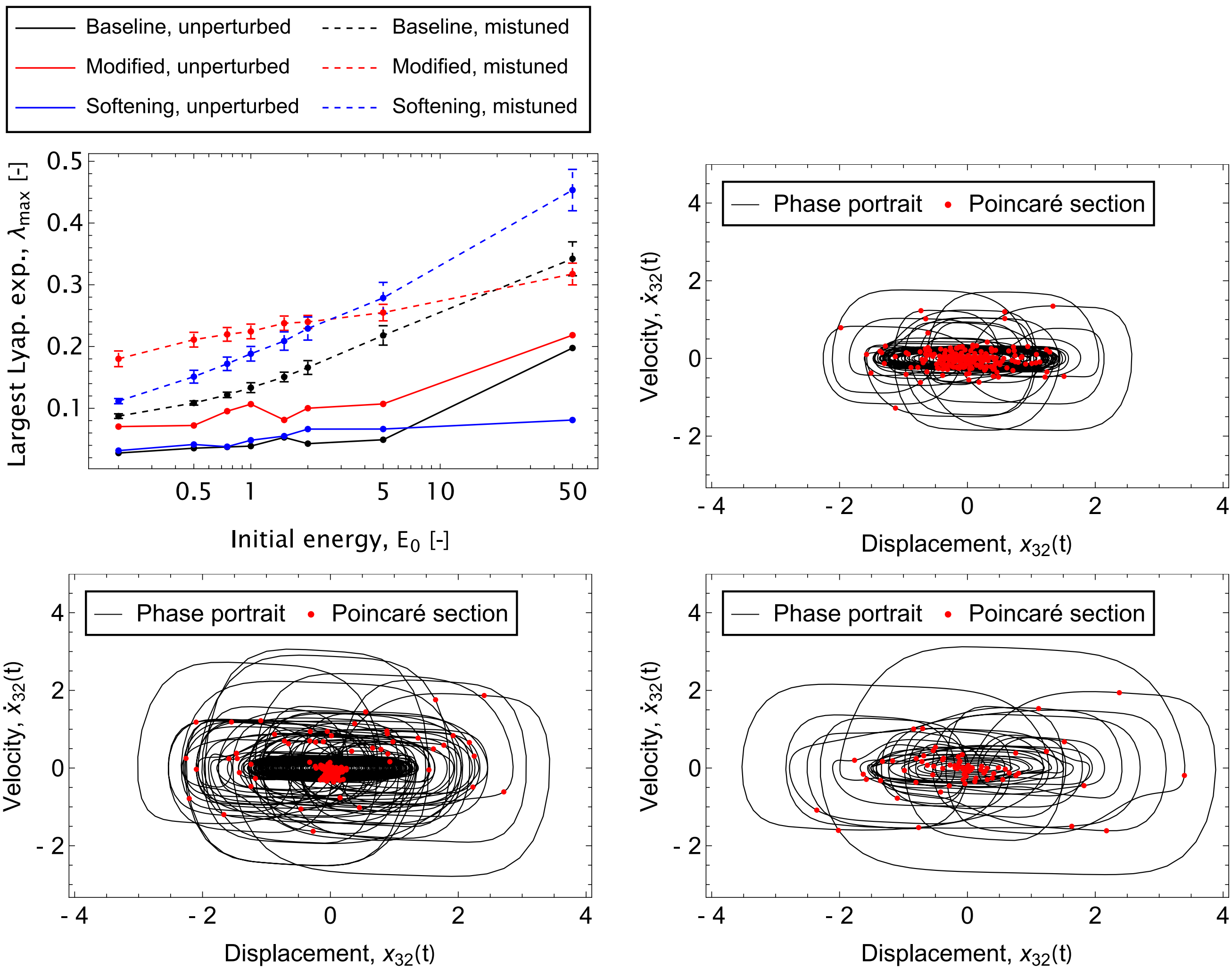

Fig. 10 Largest finite Lyapunov exponents with simple IC, and no damping at $t = 1000$, averaged over 100 realizations of perturbed systems ($r = 0.05$) (top left), representative phase portrait and Poincaré section for $x_1(t) = 0$, $\dot{x}_1(t) < 0$ for the damped unperturbed system with $E_0 = 5$ after the initial nonlinear beats of the baseline system (top right), the modified system (bottom left), and the softening system (bottom right)

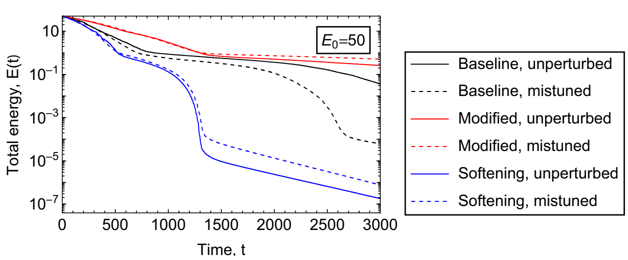

Fig. 11 Comparison of the total energy $E(t)$ for the three different parametrizations of some perturbed ($r = 0.05$) and the unperturbed systems with the simple IC for initial energy $E_0 = 50$

thus, these block masses start to oscillate in-phase. The initial energy is distributed equally between the first two levels, i.e., $E_1(0) = E_2(0)$. The in-phase IC could potentially facilitate the excitation of the in-phase NNM in contrast to the simple IC discussed in the previous section.

Fig. 13 shows the total energy $E(t)$ time histories of the unperturbed and some perturbed (with $r = 0.05$) systems for $E_0 = 1$ and $E_0 = 5$. This time the modified system with lightweight masses exhibit inarguably the strongest dissipation for $E_0 = 1$. However, as the initial energy is increased (e.g., to $E_0 = 5$) the modified system loses its efficacy compared to the baseline system. Figure 14 supports this claim as the total energy dissipated by the modified system sharply decreases for increasing initial energy. The softening system again provides high dissipation consistently over the investigated initial energy range $E_0 \in [0.2, 50]$, mostly outperforming the two other cases.

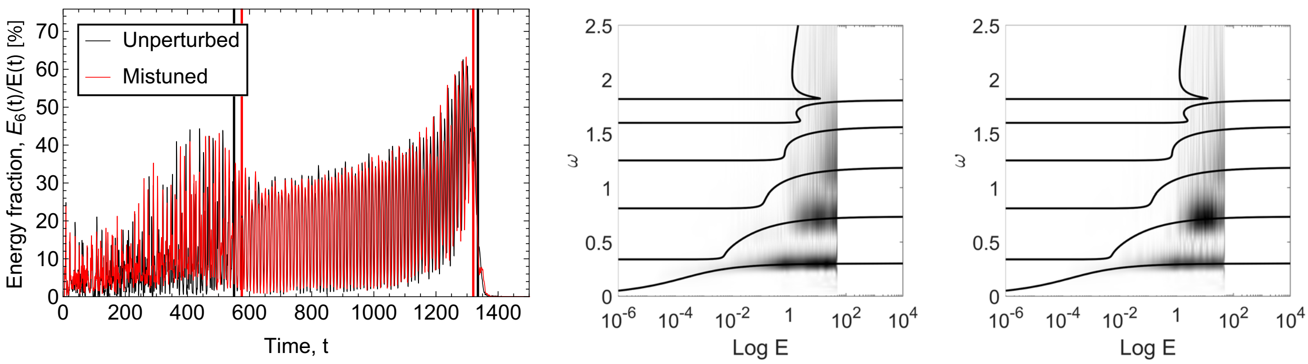

Fig. 12 Energy fraction $E_6(t)/E(t)$ stored in the last level (left), the corresponding WT of $x_{32}(t)$ for the unperturbed system (middle), and the perturbed system with $r = 0.05$ (right) for the softening system, with the simple IC and initial energy $E_0 = 50$

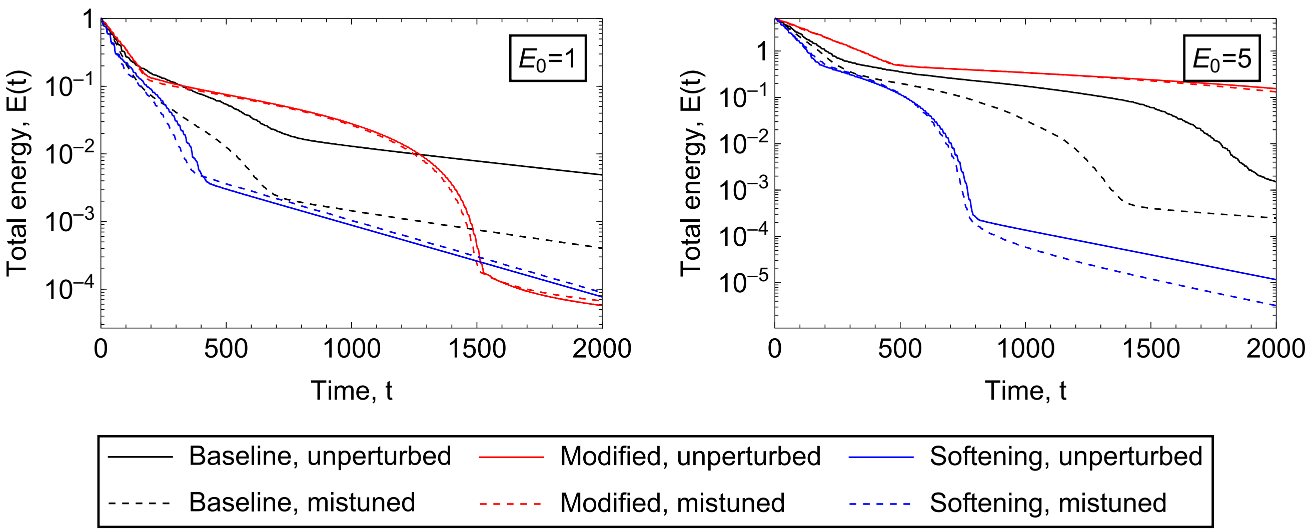

Fig. 13 Comparison of the total energy $E(t)$ for the three different parametrizations of some perturbed ($r = 0.05$) and the unperturbed systems with the in-phase IC for initial energies $E_0 = 1$ and $E_0 = 5$

In Figs. 15, 16, and 17 the energy fraction $E_6(t)/E(t)$ stored in the NES blocks and the WT of $x_{32}(t)$ superimposed onto the FEP are shown for each investigated case with $E_0 = 1$. In Figs. 18, 19, and 20 the same results are shown for $E_0 = 5$.

The unperturbed baseline system has a weak TET after the initial nonlinear beats for both $E_0 = 1$ and $E_0 = 5$, similarly to what was observed with the simple IC in Section 4.1. Interestingly, the introduction of mass mistuning not only increases the energy content stored in the NESs, but also brings the system close to fundamental TET for $E_0 = 5$. The WT plots also show complex modal interactions for the perturbed baseline system, which do not develop for the modified and the softening systems. Thus, the baseline system is the most sensitive to the perturbation of the block masses which was the case for the simple IC as well in Section 4.1.

In case of the modified system, the more efficient energy dissipation for $E_0 = 1$ is attributed to the strong, fundamental in-phase TET characterized by the increasing energy content stored in the NESs, which ceases at $t \approx 1500$. The WT plot exhibits minimal blur, indicating nearly undisturbed excitation of the two NNMs that oscillate with the lowest frequencies. This suggests minimal involvement of other higher frequency NNMs and any subharmonic NNMs that could potentially disturb the dynamics preventing efficient TET through 1:1 transient resonance capture. The two NNMs "compete" during the initial nonlinear beats. The higher frequency NNM dies when approximately 90% of the initial energy is dissipated. The in-phase NNM remains active yielding the observed in-phase fundamental TET.

Note that the NNM branches depicted on the FEP of the modified system are shifted toward lower energy levels compared to those of the baseline and the softening systems. This is why the performance of the modified system is limited at higher initial energies, it is a design that tend to perform better at low energy levels. While fundamental in-phase TET actually triggers in the modified system even at $E_0 = 5$, its slow build-up prevents rapid dissipation of energy.

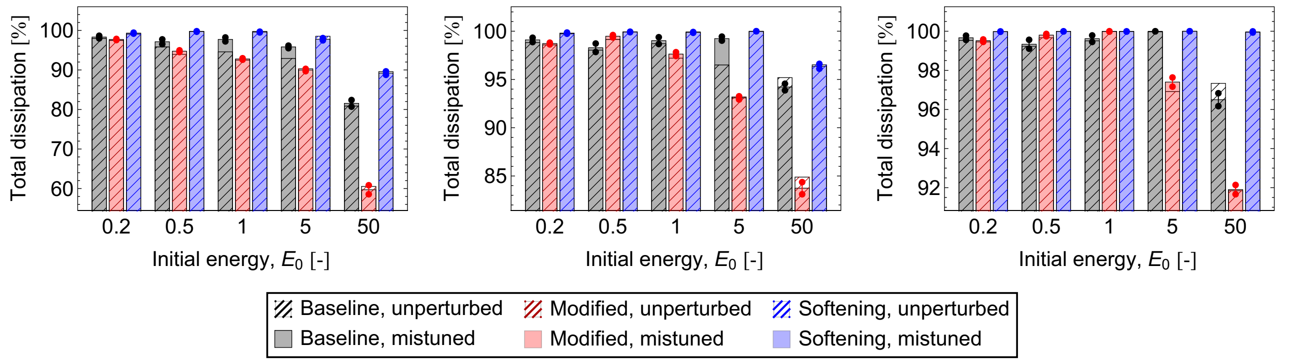

Fig. 14 Fraction of the dissipated initial energy of the system at $t = 500$ (left), $t = 1000$ (middle), and $t = 2000$ (right) as a function of the initial energy E_0 for the three different parametrizations of the unperturbed and the perturbed systems ($r = 0.05$) with in-phase IC

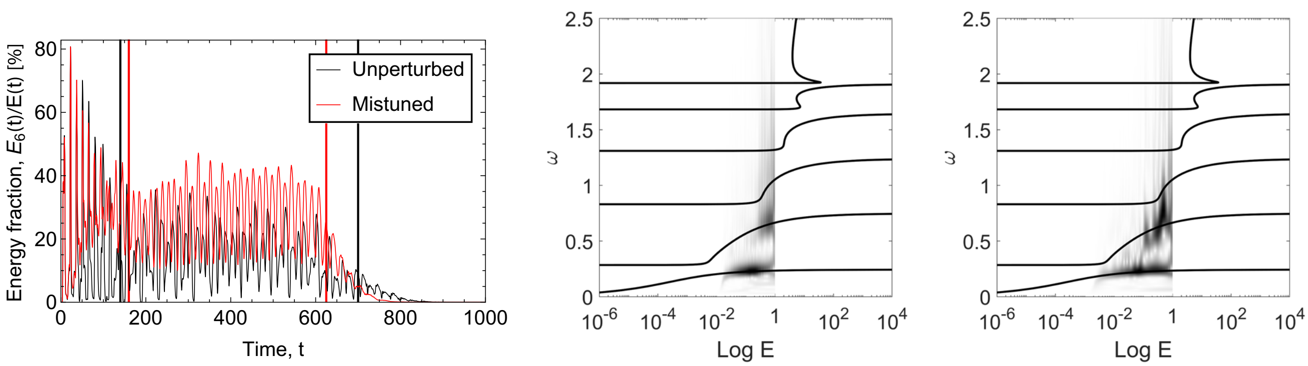

Fig. 15 Energy fraction $E_6(t)/E(t)$ stored in the last level (left), the corresponding WT of a NES block for the unperturbed system (middle), and the perturbed system with $r = 0.05$ (right) for the baseline system, with in-phase IC and initial energy $E_0 = 1$

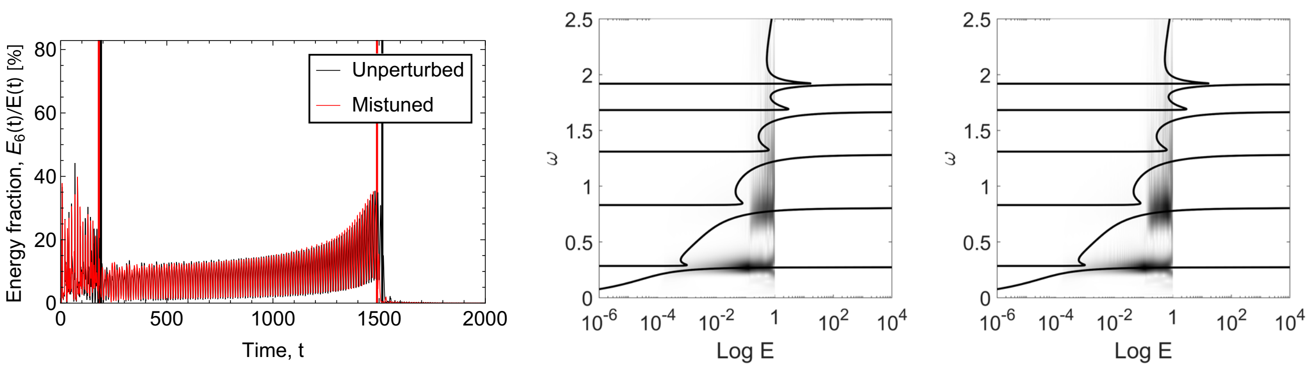

Fig. 16 Energy fraction $E_6(t)/E(t)$ stored in the last level (left), the corresponding WT of a NES block for the unperturbed system (middle), and the perturbed system with $r = 0.05$ (right) for the modified system, with in-phase IC and initial energy $E_0 = 1$

The softening system exhibits a more efficient initial nonlinear beating compared to the other two parametrizations, which is generally the case regardless of the ICs. This is why the softening system is superior in terms of energy transfer. For $E_0 = 5$, the softening system also develops efficient in-phase fundamental TET as indicated by the rapidly increasing energy content of the NESs. The emergence of fundamental TET is facilitated by the quick collapse of high-frequency modes during the initial nonlinear beats. Fig. 21 compares the evolution of the ESD of a NES block during the initial nonlinear beats for each parametrization. In the softening system the NESs couple more efficiently with the high-frequency modes, which results in a smooth, flattened spectrum by the end of the initial nonlinear beats as shown in Fig. 21. In contrast, the baseline and the modified systems preserve some of these high-frequency modes as indicated by the persisting peaks in Fig. 21. As discussed in Section 4.1 the persistence of these high-frequency modes prevent the development of strong fundamental TET. Everything considered, the results verify our assumption, that the in-phase

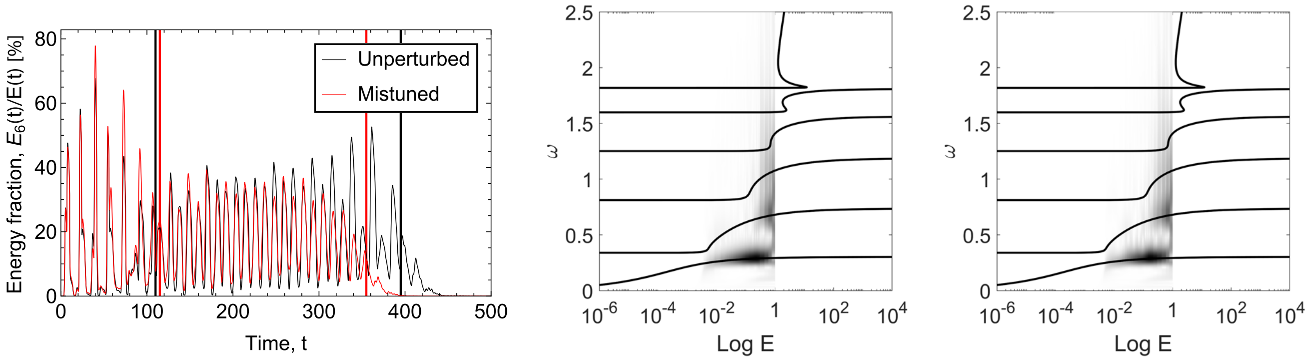

Fig. 17 Energy fraction $E_6(t)/E(t)$ stored in the last level (left), the corresponding WT of a NES block for the unperturbed system (middle), and the perturbed system with $r = 0.05$ (right) for the softening system, with in-phase IC and initial energy $E_0 = 1$

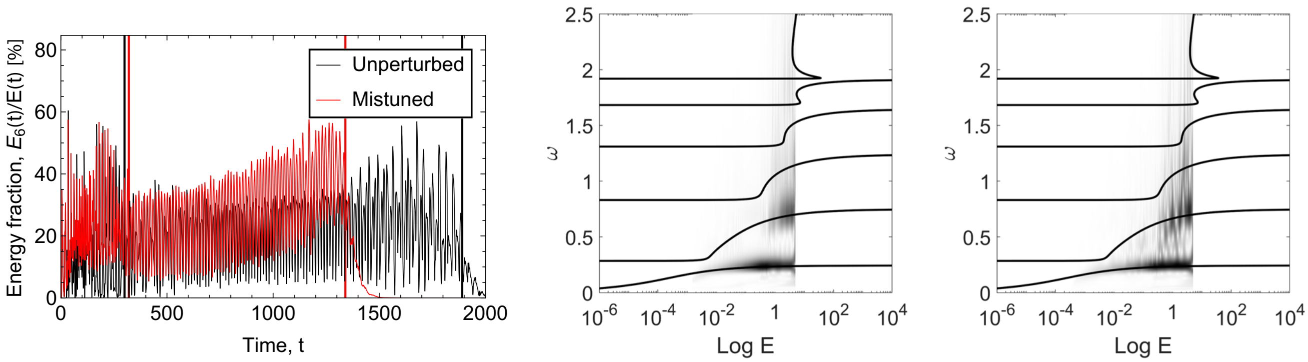

Fig. 18 Energy fraction $E_6(t)/E(t)$ stored in the last level (left), the corresponding WT of a NES block for the unperturbed system (middle), and the perturbed system with $r = 0.05$ (right) for the baseline system, with in-phase IC and initial energy $E_0 = 5$

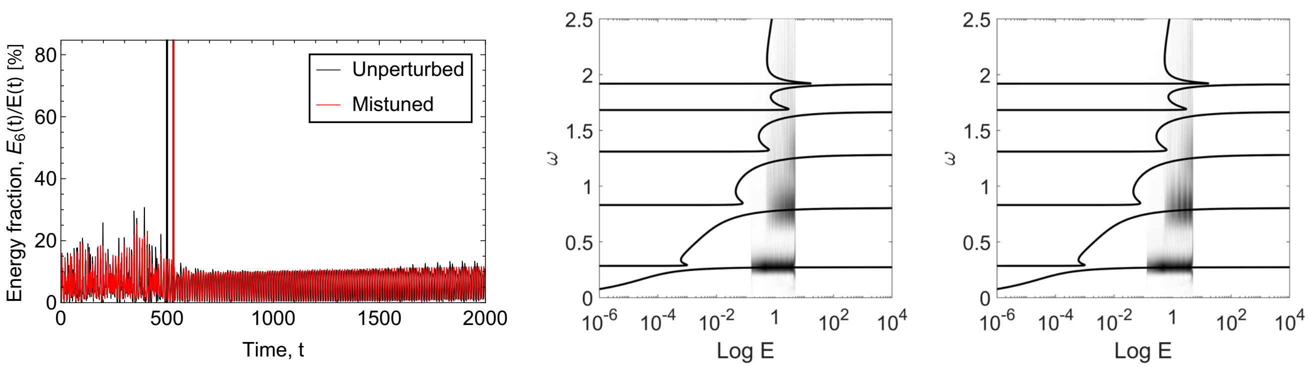

Fig. 19 Energy fraction $E_6(t)/E(t)$ stored in the last level (left), the corresponding WT of a NES block for the unperturbed system (middle), and the perturbed system with $r = 0.05$ (right) for the modified system, with in-phase IC and initial energy $E_0 = 5$

IC supports the excitation of the in-phase NNM. Strong, fundamental TET developed in multiple investigated cases with the in-phase IC, while the dynamics of the system was dominated by the in-phase NNM.

The largest Lyapunov exponents $\lambda_{\max}$ depicted in Fig. 22 again show that the $\lambda_{\max}$ values are always positive, and they are also consistently and significantly larger for all of the perturbed cases. The corresponding phase portraits and Poincaré sections also support the presence of chaos.

At the highest investigated initial energy $E_0 = 50$, the $\lambda_{\max}$ of the unperturbed system sometimes jumps an order of magnitude. This indicates that for increasing initial energy, the effect of the mistuning might be less influential, since the measured degree of chaos is already high for the unperturbed system. To verify this, the total energy $E(t)$ of the unperturbed and perturbed systems for $E_0 = 50$ are shown in Fig. 23. One can see that the mistuning indeed barely affects the affinity to dissipate vibrational energy for such a high initial energy, regardless of the parametrization of the system.

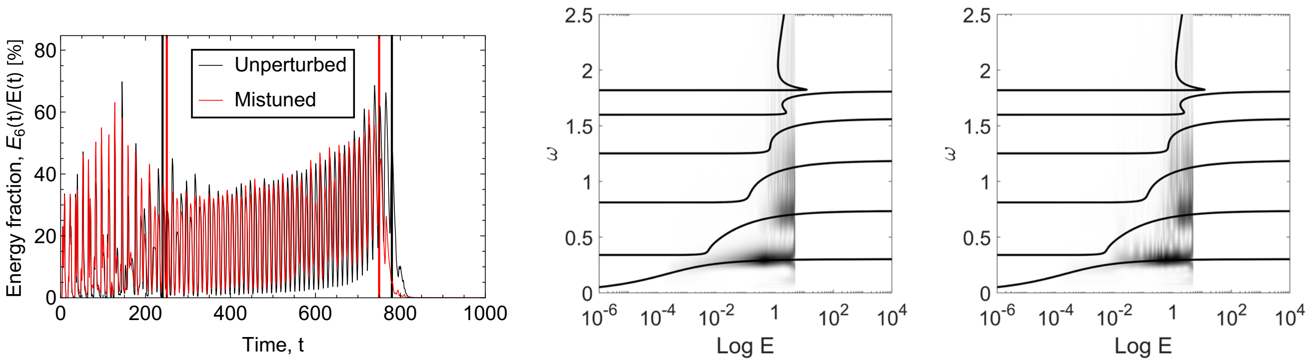

Fig. 20 Energy fraction $E_6(t)/E(t)$ stored in the last level (left), the corresponding WT of a NES block for the unperturbed system (middle), and the perturbed system with $r = 0.05$ (right) for the softening system, with in-phase IC and initial energy $E_0 = 5$

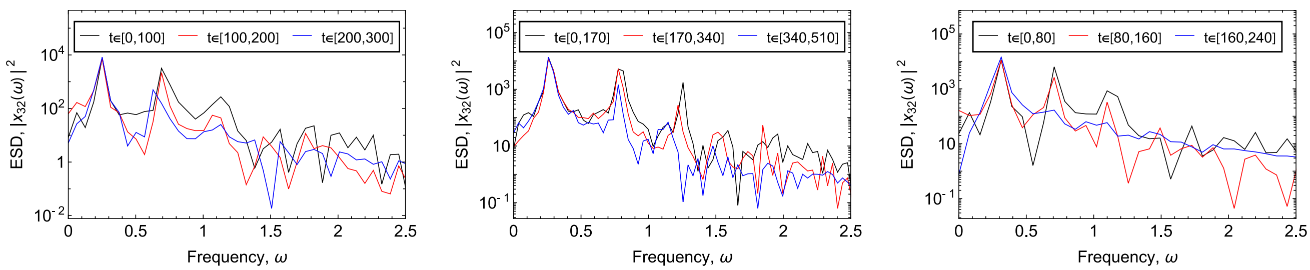

Fig. 21 Energy spectral density of the displacement $x_{32}(t)$ for the baseline system (left), modified system (middle), and softening system (right) during the initial nonlinear beats with in-phase IC, initial energy $E_0 = 5$ and no mistuning

4.3 Dynamics for mixed IC

In this case the top three blocks in the first two levels again have a nonzero initial velocity, while every other IC is zero. However, this time the sign of the initial velocity $v_{3,0}$ is negative, while both $v_{1,0}$ and $v_{2,0}$ are positive. This means that the initial phases of the two parallel blocks in the second level are opposites of each other. The initial energy is again distributed equally between the first two levels, i.e., $E_1(0) = E_2(0) = 0$. In contrast with the in-phase IC, this IC is expected to excite multiple NNMs, including modes that are hidden from the symmetric in-phase IC.

Fig. 24 shows the total energy $E(t)$ time histories of the unperturbed and some perturbed (with $r = 0.05$) systems for $E_0 = 1$ and $E_0 = 5$. For this IC, both the modified and the softening systems promote energy dissipation in comparison with the baseline system. The dissipation is once more the most efficient in case of the softening system. While the modified system outperforms the baseline system in the midrange $E_0 \in [1, 5]$, it fails to keep up with the other two systems for large initial energies, as shown by Figure 25.

In Figs. 26, 27, and 28 the energy fraction $E_6(t)/E(t)$ stored in the NES blocks and the WT of $x_{32}(t)$ superimposed onto the FEP are shown for each investigated case with $E_0 = 5$.

Once again, the mistuning has the most impact on the baseline system. Complex modal interactions can be observed on the WTs shown in Fig. 26 corresponding to the baseline system. While the mistuning does not promote the second phase of energy transfer to fundamental TET, it helps sustaining a somewhat stronger TET compared to the unperturbed case.

The modified system with lightweight NES blocks exhibits a spectacular beating between two NNMs after the initial nonlinear beats. The modulation caused by this beating can be seen on the graph of the energy fraction stored in the NESs. The signature of this phenomenon can also be seen on the wavelet plot as a "barcode" pattern. The presence of beating is verified by the displacement solutions $x_{16}(t)$ and $x_{32}(t)$ seen in Fig. 29, as well as the corresponding ESD plots, which show that there are two strongly activated modes with similar frequencies during the second TET phase. This beating of the two NNMs is so dominant that even the moderate mistuning with $r = 0.05$ does not affect it. In Bak et al. [38] it is discussed that for this type of IC, where some blocks start to oscillate in an out-of-phase fashion, a NNM activates with an oscillation frequency being very close to that of the in-phase NNM causing the observed beating phenomenon. For the entire investigated initial energy range $E_0 \in [0.2, 50]$ this beating phenomenon induces the second TET phase in the modified system. This dynamics is characteristic to the binary tree structure of the system, as the beating phenomenon cannot be triggered without providing different initial conditions for parallel blocks.

Still, the softening system remains superior in terms of dissipation, because its initial nonlinear beats are much more

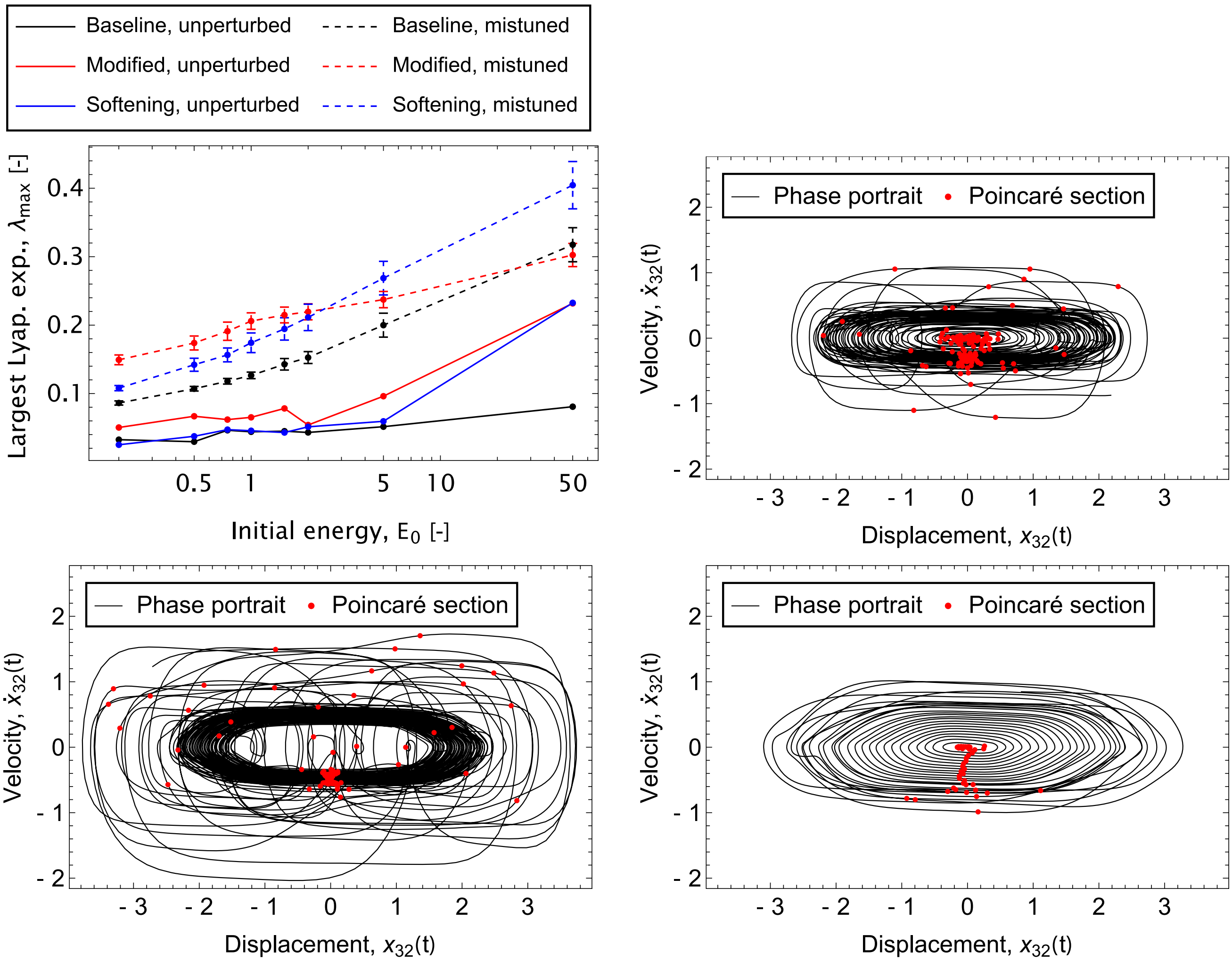

Fig. 22 Largest finite Lyapunov exponents with in-phase IC, and no damping at $t = 1000$, averaged over 100 realizations of perturbed systems ($r = 0.05$) (top left), the phase portrait and Poincaré section for $x_1(t) = 0, \dot{x}_1(t) < 0$ for the damped unperturbed system with $E_0 = 5$ after the initial nonlinear beats in the baseline system (top right), the modified system (bottom left), and the softening system (bottom right)

efficient compared to those of the baseline and modified systems as discussed earlier in Section 4.2. The increased dissipation rate of the perturbed softening system is facilitated by even stronger initial nonlinear beats. For the lower energy level $E_0 = 1$, perturbation of the block masses is required to achieve a second phase of TET after the initial nonlinear beats as it is not triggered in the unperturbed system, similarly to what happened with the simple IC.

The largest Lyapunov exponents λ_{max} shown in Fig. 30 are again positive in every case, and they are consistently and significantly larger for all of the perturbed cases. The representative phase portraits and Poincaré sections depicted in Fig. 30 are also consistent with the chaotic dynamics indicated by the positive Lyapunov exponents. At the highest investigated initial energy $E_0 = 50$, the largest Lyapunov exponent of the unperturbed softening system exhibit a sharp

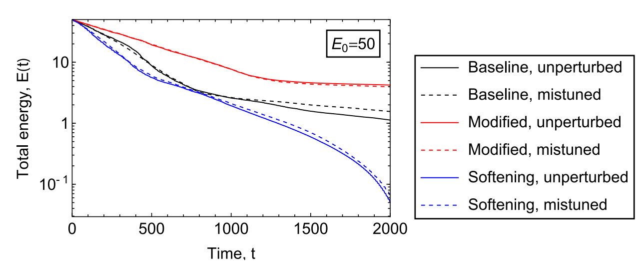

Fig. 23 Comparison of the total energy $E(t)$ for the three different parametrization of some perturbed ($r = 0.05$) and the unperturbed systems with the in-phase IC for initial energy $E_0 = 50$

increase, reaching the range of the largest Lyapunov exponents corresponding to the perturbed cases, indicating that the effects of the mistuning might be less significant in this case.

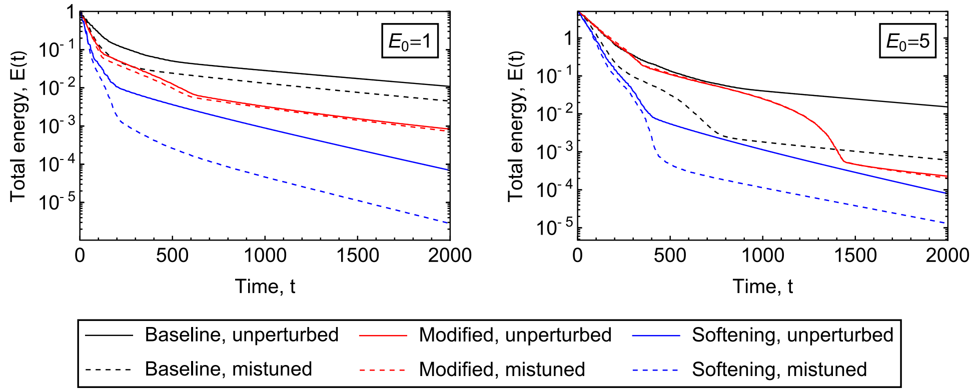

Fig. 24 Comparison of the total energy $E(t)$ for the three different parametrization of some perturbed ($r = 0.05$) and the unperturbed systems with the mixed IC for initial energies $E_0 = 1$ and $E_0 = 5$

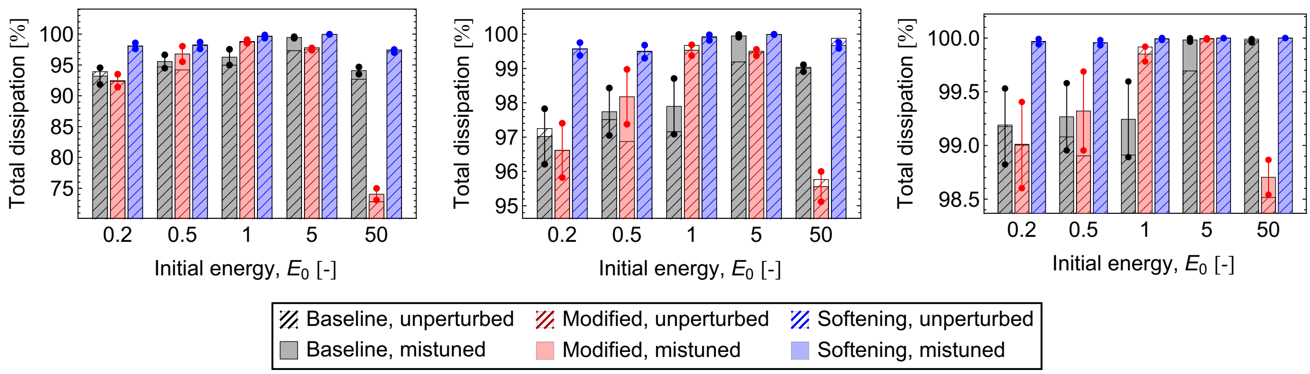

Fig. 25 Fraction of the dissipated initial energy of the system at $t = 500$ (left), $t = 1000$ (middle), and $t = 2000$ (right) as a function of the initial energy E_0 for the three different parametrizations of the unperturbed and the perturbed systems ($r = 0.05$) with mixed IC

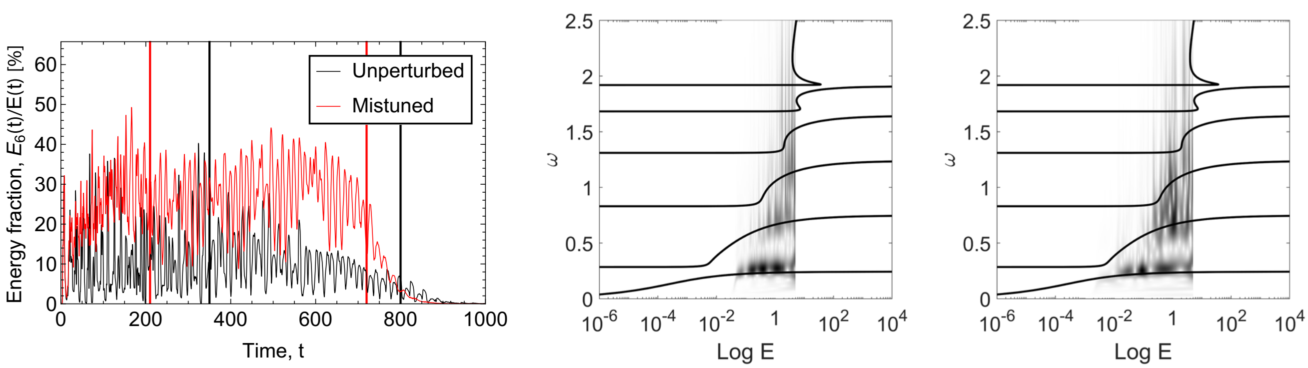

Fig. 26 Energy fraction $E_6(t)/E(t)$ stored in the last level (left), the corresponding WT of a NES block for the unperturbed system (middle), and the perturbed system with $r = 0.05$ (right) for the baseline system, with mixed IC and initial energy $E_0 = 5$

The total energy $E(t)$ for the largest investigated initial energy $E(0) = 50$ depicted in Fig. 31 shows once again that the performance of the softening system remains convincing for an order of magnitude higher initial energy. Moreover, now the softening system also exhibits the beating that was a characteristic of the modified system as shown in Fig. 32. As emphasized earlier based on the evolution of the largest Lyapunov exponents as function of the initial energy, the mistuning indeed has no significant impact for such a large initial energy. We conclude that the perturbation of the block masses has a diminishing effect on the dynamics as the initial energy increases.

5 Summary and discussion

A MDoF nonlinear binary tree-structured oscillator was introduced, in which NESs comprised the leaves of the tree. Different parametrizations for the block masses and spring stiffnesses were proposed and the response of the system was studied for different types of initial conditions. The goal was

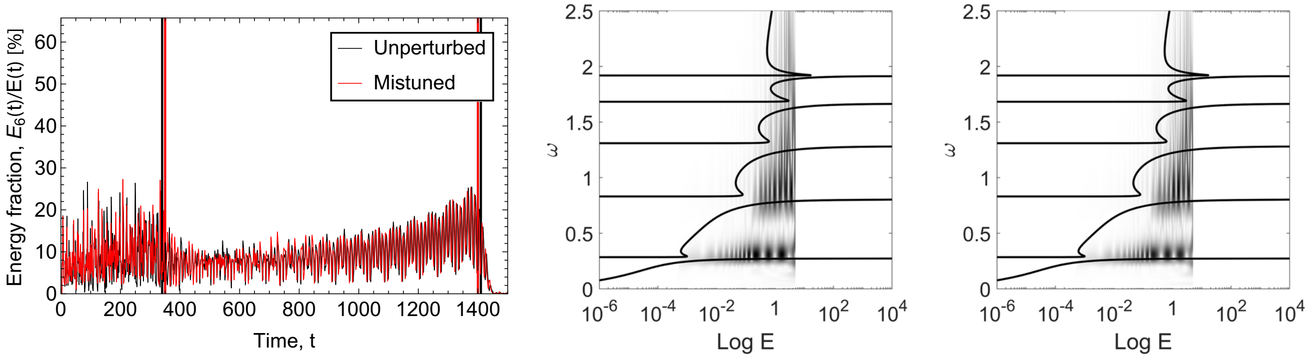

Fig. 27 Energy fraction $E_6(t)/E(t)$ stored in the last level (left), the corresponding WT of a NES block for the unperturbed system (middle), and the perturbed system with $r = 0.05$ (right) for the modified system, with mixed IC and initial energy $E_0 = 5$

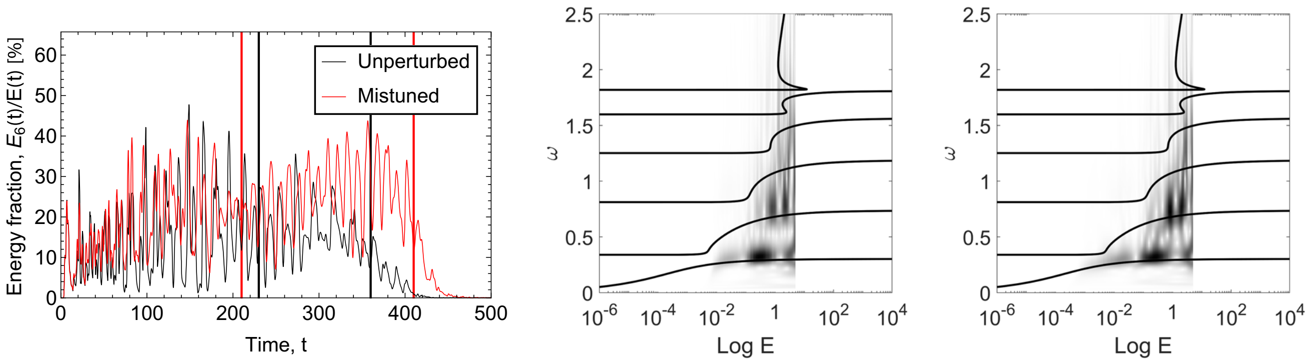

Fig. 28 Energy fraction $E_6(t)/E(t)$ stored in the last level (left), the corresponding WT of a NES block for the unperturbed system (middle), and the perturbed system with $r = 0.05$ (right) for the softening system, with mixed IC and initial energy $E_0 = 5$

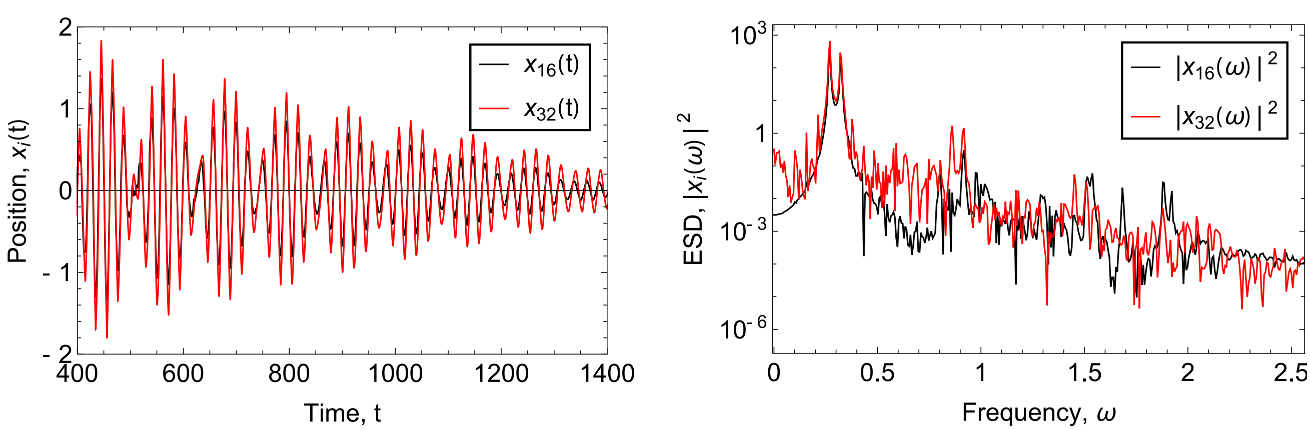

Fig. 29 Displacement solutions $x_{16}(t)$ and $x_{32}(t)$ (left) and the corresponding ESD of $x_{16}(t)$ and $x_{32}(t)$ during the second TET phase (right) for the unperturbed modified system with mixed IC and initial energy $E_0 = 5$

to investigate the ability of this system to dissipate vibrational energy over a broad input energy range with special focus on how the different parametrizations and the mistuning of the block masses affect the input energy range in which the NESs remain active.

The masses of the blocks and the stiffnesses of the springs in the system gradually decrease as the tree branches, these parameters follow the simple power-law Eq. (8) as function of the tree level l. In the baseline system of the investigations the block masses and spring stiffnesses were halved on each successive level of the tree. In this system the sum of the block masses as well as the sum of the spring stiffnesses are the same for each level. Two other parametrizations were considered to promote energy dissipation. In the modified system we prescribed a local modification which further decreased the mass of the NES blocks yielding a modified system with

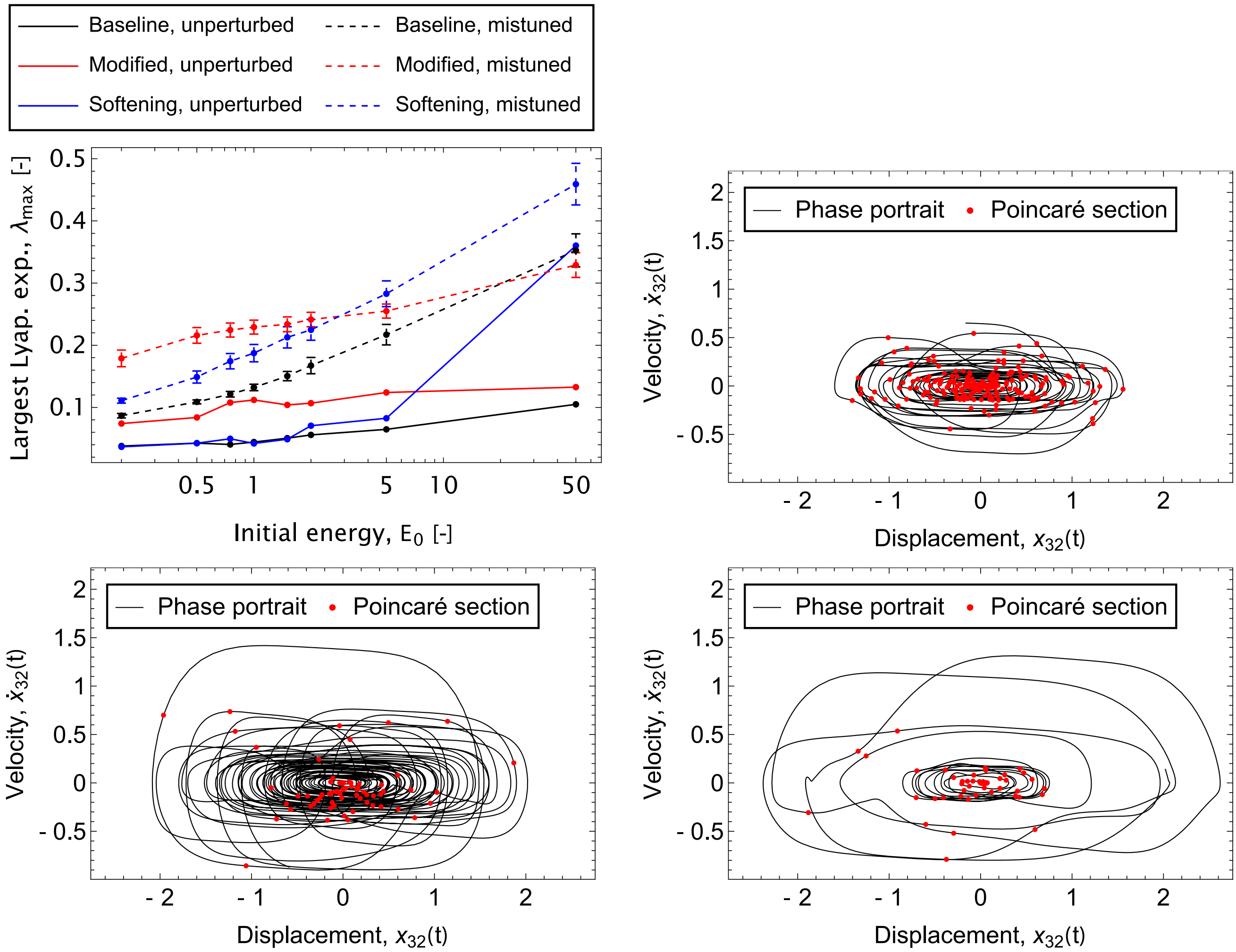

Fig. 30 Largest finite Lyapunov exponents with mixed IC, and no damping at $t = 1000$, averaged over 100 realizations of perturbed systems ($r = 0.05$) (top left), the phase portrait and Poincaré section for $x_1(t) = 0$, $\dot{x}_1(t) < 0$ for the damped unperturbed system with $E_0 = 5$ after the initial nonlinear beats in the baseline system (top right), the modified system (bottom left), and the softening system (bottom right)

lightweight NESs. In contrast, the so-called softening system has completely different parameters as the scaling parameter σ was decreased, yielding softer connections and lighter block masses across the levels of the tree compared to the baseline system.

In general, the baseline system exhibited only a weak second TET phase after the initial nonlinear beats without perturbation. We detected residual energy content in some high-frequency modes that prevented clear 1:1 transient resonance capture. We found that reducing the mass of the NES blocks worked better than the baseline system in some cases for smaller input energy levels, which is in agreement with our previous study [38]. We assumed that the in-phase and mixed ICs could force the system into a more efficient form of TET through the excitation of the in-phase NNM and some hidden modes, respectively. The modified system reacted to the ICs as per our initial expectation, and exhibited a strong

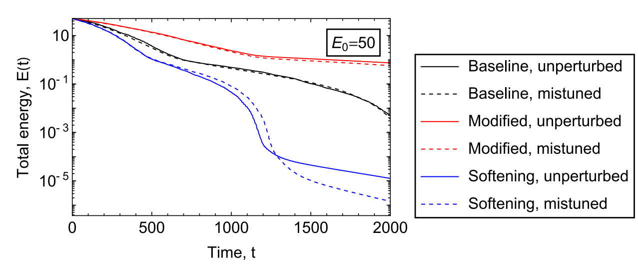

Fig. 31 Comparison of the total energy $E(t)$ for the three different parametrization of some perturbed ($r = 0.05$) and the unperturbed systems with the mixed IC for initial energy $E_0 = 50$

second TET phase driven by different mechanisms. In particular, we managed to trigger in-phase fundamental TET caused by the NESs engaging with the in-phase NNM, as well as a similarly strong TET caused by a beating of two NNMs having slightly different oscillation frequencies in the

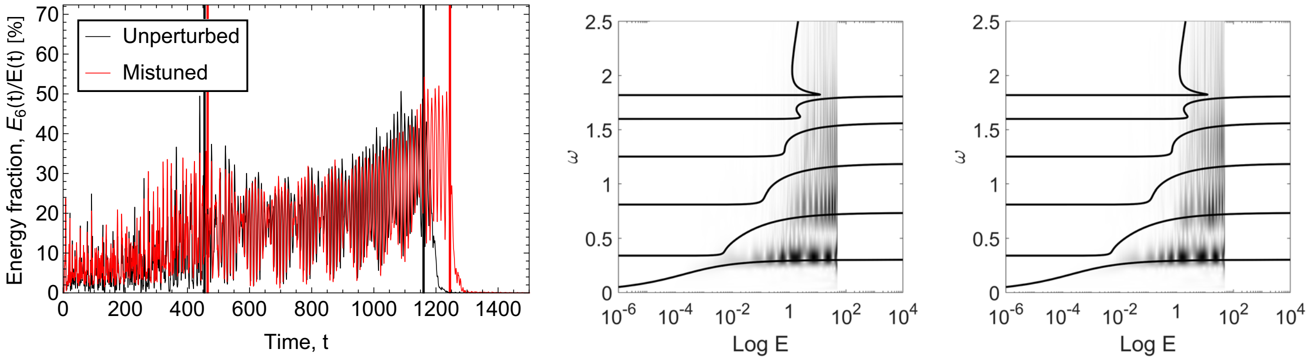

Fig. 32 Energy fraction $E_6(t)/E(t)$ stored in the last level (left), the corresponding WT of a NES block for the unperturbed system (middle), and the perturbed system with $r = 0.05$ (right) for the softening system, with mixed IC and initial energy $E_0 = 50$

modified system. However, this modified system performed poorly in terms of dissipation for larger input energies.The decrease of the mass of the NES blocks alters the FEP of the system by essentially displacing all NNM branches toward lower energy levels. This implies that such a design is suitable to increase the efficacy of energy transfer and dissipation for lower input energies, but cannot extend the range of input energy in which the NESs perform well. In terms of energy transfer and dissipation, the softening system consistently outperformed both the baseline and the modified systems for the entire investigated range of input energy levels. In general, the initial nonlinear beats proved to be very effective with the softer connections and lighter block masses, and fundamental TET also developed for larger initial energies. The underlying reason for the superior behavior of the softening system was found to be its affinity to quickly reduce the energy content of the high-frequency modes providing favorable conditions for the onset of strong fundamental TET. The conclusion is that such a design can extend the range of input energy in which the NESs perform well.

The mistuning of the block masses promoted chaotic dynamics indicated by the sharp increase of the calculated largest Lyapunov exponents — which were positive in every investigated case — compared to those of the unperturbed system. In most cases, the perturbation of the block masses yielded the localization of increased amount of vibrational energy in the NESs (shown by the graphs of $E_6(t)/E(t)$). Thus, the dissipation of the vibrational energy of the system was typically more efficient with mistuned block masses. However, the impact of the mistuning was diminishing for increased input energy. The takeaway is that small or moderate perturbation of the block masses intensifies the energy transfer and the dissipation of vibrational energy only up to a certain threshold energy level.

Everything considered, the results of this study showcased that certain parametrizations of MDoF oscillators can extend the range of input energy for which simple NESs remain effective at dissipating the vibrational energy of the system. On top of that the perturbation of the block masses have potential to further increase the dissipative performance via the promotion of chaotic interactions between the NNMs of the system. In future works, we aim to extend this paper's investigations to continuous excitations of the largest block mass. We also plan to examine the effects of different random distributions used for the mistuning of the masses. We also intend to study the separation of NNMs, which was conjectured to occur in some of the cases presented in this paper. Further study of the binary tree-structured oscillator may facilitate development of more efficient vibration suppressors, as well as motivate broader research into systems with multiple parallel NES blocks. Continued research into the random mistuning of system parameters offers further possibilities towards improved vibration reduction. A long term prospect of the model is the development of a new variant of the turbulent shell models [49] with the incorporation of velocity-dependent nonlinear dampers, opening up the possibility to relate certain aspects of the model with turbulent flows.

Author Contributions R.R.: Writing - review & editing, Writing – original draft, Visualization, Methodology, Investigation, Project administration. B.D.B.: Writing - review & editing, Writing – original draft, Visualization, Methodology, Conceptualization, Investigation, Supervision, Resources.

Funding Open access funding provided by Budapest University of Technology and Economics. The research reported in this paper is part of project no. TKP-6-6/PALY-2021. Project no. TKP-6-6/PALY-2021 has been implemented with the support provided by the Ministry of Culture and Innovation of Hungary from the National Research, Development and Innovation Fund, financed under the TKP2021-NVA funding scheme. This work has been supported by the Hungarian National Research, Development and Innovation Fund under contract NKFI K 137726. One of the authors, Bendegúz Dezső Bak has been supported by the Bolyai Research Scholarship of the Hungarian Academy of Sciences (MTA).
The project supported by the Doctoral Excellence Fellowship Programme (DCEP) is funded by the National Research Development and Innovation Fund of the Ministry of Culture and Innovation and the Budapest University of Technology and Economics.

Data Availability The datasets generated during and/or analyzed during the current study are available from the corresponding author on reasonable request.

Declarations

Conflicts of Interest The authors have no relevant financial or non-financial interests to disclose. The authors have no conflicts of interest to declare that are relevant to the content of this article. All authors certify that they have no affiliations with or involvement in any organization or entity with any financial interest or non-financial interest in the subject matter or materials discussed in this manuscript. The authors have no financial or proprietary interests in any material discussed in this article.

References

1. Vakakis, A.F., Gendelman, O.V., Bergman, L.A., Mojahed, A., Gzal, M.: Nonlinear targeted energy transfer: state of the art and new perspectives. Nonlinear Dyn. **108**(2), 711–741 (2022)
2. Li, S.B., Ding, H.: Effective damping zone of nonlinear energy sinks. Nonlinear Dyn. **111**(20), 18605–18629 (2023)
3. Geng, X.F., Ding, H.: Theoretical and experimental study of an enhanced nonlinear energy sink. Nonlinear Dyn. **104**(4), 3269–3291 (2021)
4. Zhang, Z., Gao, Z.T., Fang, B., Zhang, Y.W.: Vibration suppression of a geometrically nonlinear beam with boundary inertial nonlinear energy sinks. Nonlinear Dyn. **109**(3), 1259–1275 (2022)
5. Dang, W., Liu, S., Chen, L., Yang, T.: A dual-stage inerter-enhanced nonlinear energy sink. Nonlinear Dyn. **111**(7), 6001–6015 (2023)
6. Dou, J., Yao, H., Li, H., Cao, Y., Liang, S.: Vibration suppression of multi-frequency excitation using cam-roller nonlinear energy sink. Nonlinear Dyn. **111**(13), 11939–11964 (2023)
7. Jin, Y., Hou, S., Yang, T.: Cascaded essential nonlinearities for enhanced vibration suppression and energy harvesting. Nonlinear Dyn. **103**(2), 1427–1438 (2021)
8. Franzini, G.R., Maciel, V.S.F., Vernizzi, G.J., Zulli, D.: Simultaneous passive suppression and energy harvesting from galloping using a bistable piezoelectric nonlinear energy sink. Nonlinear Dyn. **111**(24), 22215–22236 (2023)
9. Li, H., Li, S., Ding, Q., Xiong, H., Kong, X.: An electromagnetic vibro-impact nonlinear energy sink for simultaneous vibration suppression and energy harvesting in vortex-induced vibrations. Nonlinear Dyn. **112**(8), 5919–5936 (2024)
10. Vakakis, A.F., Gendelman, O.V., Bergman, L.A., McFarland, D.M., Kerschen, G., Lee, Y.S.: Nonlinear Targeted Energy Transfer in Mechanical and Structural Systems. Berlin, Springer Science & Business Media (2008)
11. Borges, R.A., de Lima, A.M.G., Steffen, V., Jr.: Robust optimal design of a nonlinear dynamic vibration absorber combining sensitivity analysis. Shock. Vib. **17**(4–5), 507–520 (2010)
12. Zhou, D., Huang, D.: Stochastic response analysis and robust optimization of nonlinear turbofan engine system. Nonlinear Dyn. **110**(3), 2225–2245 (2022)
13. Habib, G., Romeo, F.: The tuned bistable nonlinear energy sink. Nonlinear Dyn. **89**(1), 179–196 (2017)
14. Gendelman, O., Manevitch, L., Vakakis, A.F., M'Closkey, R.: Energy pumping in nonlinear mechanical oscillators: part I-dynamics of the underlying Hamiltonian systems. J. Appl. Mech. **68**(1), 34–41 (2001)
15. Vakakis, A.F., Gendelman, O.: Energy pumping in nonlinear mechanical oscillators: part II-resonance capture. J. Appl. Mech. **68**(1), 42–48 (2001)
16. Ding, H., Chen, L.Q.: Designs, analysis, and applications of nonlinear energy sinks. Nonlinear Dyn. **100**(4), 3061–3107 (2020)
17. Al-Shudeifat, M.A., Saeed, A.S.: Frequency-energy plot and targeted energy transfer analysis of coupled bistable nonlinear energy sink with linear oscillator. Nonlinear Dyn. **105**(4), 2877–2898 (2021)
18. Zeng, Y.C., Ding, H., Du, R.H., Chen, L.Q.: Micro-amplitude vibration suppression of a bistable nonlinear energy sink constructed by a buckling beam. Nonlinear Dyn. **108**(4), 3185–3207 (2022)
19. Wang, T., Ding, Q.: Targeted energy transfer analysis of a nonlinear oscillator coupled with bistable nonlinear energy sink based on nonlinear normal modes. J. Sound Vib. **556**, 117727 (2023)
20. Li, H., Li, A., Kong, X., Xiong, H.: Dynamics of an electromagnetic vibro-impact nonlinear energy sink, applications in energy harvesting and vibration absorption. Nonlinear Dyn. **108**(2), 1027–1043 (2022)
21. Wu, Z., Paredes, M., Seguy, S.: Targeted energy transfer in a vibro-impact cubic NES: description of regimes and optimal design. J. Sound Vib. **545**, 117425 (2023)
22. Liu, R., Kuske, R., Yurchenko, D.: Maps unlock the full dynamics of targeted energy transfer via a vibro-impact nonlinear energy sink. Mech. Syst. Signal Process. **191**, 110158 (2023)
23. Chen, J.E., Theurich, T., Krack, M., Sapsis, T., Bergman, L.A., Vakakis, A.F.: Intense cross-scale energy cascades resembling "mechanical turbulence" in harmonically driven strongly nonlinear hierarchical chains of oscillators. Acta Mech. **233**(4), 1289–1305 (2022)
24. Chen, J.E., Sun, M., Zhang, W., Li, S., Wu, R.: Cross-scale energy transfer of chaotic oscillator chain in stiffness-dominated range. Nonlinear Dyn. **110**(3), 2849–2867 (2022)
25. da Silva, J.A.I., Marques, F.D.: Multi-degree of freedom nonlinear energy sinks for passive control of vortex-induced vibrations in a sprung cylinder. Acta Mech. **232**(10), 3917–3937 (2021)
26. Liu, Y., Wang, Y.: Vibration suppression of a linear oscillator by a chain of nonlinear vibration absorbers with geometrically nonlinear damping. Commun. Nonlinear Sci. Numer. Simul. **118**, 107016 (2023)
27. Kumar, R.K., Kumar, A.: Vibration suppression and stability analysis of a beam at large amplitude excitation using a two-degree-of-freedom nonlinear energy sink. Acta Mech. **235**(2), 971–990 (2024)
28. Yang, T., Dang, W., Chen, L.: Two-dimensional inerter-enhanced nonlinear energy sink. Nonlinear Dyn. **112**(1), 379–401 (2024)
29. Zhang, Y., Liang, Y., Zhang, X., Chen, Z., Kong, X.: Vibration characteristics analysis of a new 2-dof nonlinear energy sink considering frequency detuning. J. Vib. Eng. Technol. **14**(2), 74 (2026)
30. Loong, C.N., Dimitrakopoulos, E.G.: Recursive modal properties of fractal monopodial trees, from finite to infinite order. J. Sound Vib. **595**, 118770 (2025)

31. Kovacic, I., Zukovic, M., Radomirovic, D.: On a localization phenomenon in two types of bio-inspired hierarchically organized oscillatory systems. Nonlinear Dyn. **99**(1), 679–706 (2020)
32. Richardson, L.F.: Weather Prediction by Numerical Process. Cambridge University Press (1922)
33. Kolmogorov, A.N.: The local structure of turbulence in incompressible viscous fluid for very large Reynolds numbers. Doklady Akademiya Nauk SSSR **30**(4), 301–305 (1941)
34. Vakakis, A.F.: Passive nonlinear targeted energy transfer. Phil. Trans. R. Soc. A **376**(2127), 20170132 (2018)
35. Boudaoud, A., Cadot, O., Odille, B., Touzé, C.: Observation of wave turbulence in vibrating plates. Phys. Rev. Lett. **100**(23), 234504 (2008)
36. Kalmár-Nagy, T., Bak, B.D.: An intriguing analogy of Kolmogorov's scaling law in a hierarchical mass-spring-damper model. Nonlinear Dyn. **95**(4), 3193–3203 (2019)
37. Rochlitz, R., Bak, B.D., Kalmár-Nagy, T.: Self-similar eigenvalue distribution of a binary tree-structured mass-spring-damper system. J. Sound Vib. **611**, 119111 (2025)
38. Bak, B.D., Rochlitz, R., Kalmár-Nagy, T.: Energy transfer mechanisms in binary tree-structured oscillator with nonlinear energy sinks. Nonlinear Dyn. **111**(11), 9875–9888 (2023)
39. Le, T.P., Argoul, P.: Continuous wavelet transform for modal identification using free decay response. J. Sound Vib. **277**(1–2), 73–100 (2004)
40. Zhang, G., Tang, B., Chen, Z.: Operational modal parameter identification based on PCA-CWT. Measurement **139**, 334–345 (2019)
41. Hubbard, S.A., Vakakis, A.F., Bergman, L.A., McFarland, D.M.: Construction and use of the frequency-energy plot for a system with two essential nonlinearities. In ASME 2011 International Design Engineering Technical Conferences and Computers and Information in Engineering Conference, pages 449–456, (2011)
42. Zhang, X.H.: Constructing the frequency-energy plot of nonlinear vibratory systems via the modified Lindstedt-Poincaré method. Adv. Mater. Res. **655**, 547–550 (2013)
43. Kuptsov, P.V., Parlitz, U.: Theory and computation of covariant Lyapunov vectors. J. Nonlinear Sci. **22**(5), 727–762 (2012)
44. Chen, J., Zhang, W., Liu, J., Hu, W.: Vibration absorption of parallel-coupled nonlinear energy sink under shock and harmonic excitations. Appl. Math. Mech. **42**(8), 1135–1154 (2021)
45. Gendelman, O.V., Gorlov, D.V., Manevitch, L.I., Musienko, A.I.: Dynamics of coupled linear and essentially nonlinear oscillators with substantially different masses. J. Sound Vib. **286**(1), 1–19 (2005)
46. Sigalov, G., Gendelman, O.V., Al-Shudeifat, M.A., Manevitch, L.I., Vakakis, A.F., Bergman, L.A.: Resonance captures and targeted energy transfers in an inertially-coupled rotational nonlinear energy sink. Nonlinear Dyn. **69**(4), 1693–1704 (2012)
47. Nayfeh, A.H., Mook, D.T.: Nonlinear oscillations. Wiley, New York (2008)
48. Perchikov, N., Gendelman, O.V.: Nonlinear dynamics of hidden modes in a system with internal symmetry. J. Sound Vib. **377**, 185–215 (2016)
49. Ditlevsen, P.D.: Turbulence and shell models. Cambridge University Press (2010)